

Sensor Fault Detection and Compensation with Performance Prescription for Robotic Manipulators

S. Mohammadreza Ebrahimi¹, Farid Norouzi², Hossein Dastres¹, Reza Faieghi^{*3},
Mehdi Naderi⁴, and Milad Malekzadeh⁴

¹Department of Electrical Engineering, Babol Noshirvani University of Technology, Babol, Iran

²Department of Mechanical Engineering, Babol Noshirvani University of Technology, Babol, Iran

³Department of Aerospace Engineering, Toronto Metropolitan University, Toronto, Canada

⁴School of Production Engineering and Management, Technical University of Crete, Chania, Greece

Abstract

This paper focuses on sensor fault detection and compensation for robotic manipulators. The proposed method features a new adaptive observer and a new terminal sliding mode control law established on a second-order integral sliding surface. The method enables sensor fault detection without the need to know the bounds on fault value and/or its derivative. It also enables fast and fixed-time fault-tolerant control whose performance can be prescribed beforehand by defining funnel bounds on the tracking error. The ultimate boundedness of the estimation errors for the proposed observer and the fixed-time stability of the control system are shown using Lyapunov stability analysis. The effectiveness of the proposed method is verified using numerical simulations on two different robotic manipulators, and the results are compared with existing methods. Our results demonstrate performance gains obtained by the proposed method compared to the existing results.

Keywords: Fault detection, fault-tolerant control, fixed-time stability, performance prescription, robot manipulator

1. Introduction

A fault in a robotic system can be defined as an unexpected or unplanned deviation from the normal behavior of the system, which can result in incorrect or unintended actions being taken. One of the most common types of faults is the sensor fault which occurs when a sensor fails to accurately measure a variable or provides incorrect data. As surveyed in [1], the common approach to detect sensor faults is to use state observers. Examples in the context of robotic manipulators include bank of linear observers [2], H_∞ -based observer [3], sliding mode observer and its higher-order variations [4, 5], and adaptive observer [6, 7]. One notable mention is [8] in which the sensor fault detection problem is transformed into a virtual actuator fault detection framework to use the rich body of literature on actuator fault detection and compensation [1].

*Corresponding author: reza.faieghi@torontomu.ca

Once a fault is detected, fault-tolerant control (FTC) methods are required to mitigate the effects of the fault. As pointed out in [1], one popular FTC method for nonlinear systems is sliding mode control (SMC). Examples of using SMC in FTC include the following. In [9], FTC is achieved using SMC integrated with control allocation to handle actuator faults without reconfiguring the controller. In [10], an FTC scheme for over-actuated linear systems is proposed using integral SMC and control allocation techniques. In [11], two SMC algorithms are presented for nonlinear systems with modeling uncertainties and actuator faults, followed by numerical verifications on a Boeing 747-100/200 model. In [12], two robust control methods based on integral SMC are proposed to handle actuator faults and external disturbances in spacecraft attitude dynamics. In [13], an SMC algorithm is designed for a coaxial trirotor aircraft. This algorithm has proven to be effective in handling defects and uncertainties in the system. In [14], an SMC-based scheme for fault detection and FTC of motor systems is explored under various faults and disturbances. In [15], actuator FTC is achieved for a coaxial octorotor uncrewed aerial vehicle using radial basis function networks, fuzzy logic, and SMC. In [16], a passive SCM-based FTC is proposed for the dynamic positioning of ships in the presence of actuator faults, parameter uncertainties, and external disturbances. In [17], SMC is integrated with self-tuning proportional-integral-derivative control to achieve FTC for robotic manipulators. Overall, SMC offers simplicity, flexibility for integration with different techniques, and robustness. The latter provides passive fault tolerance properties, especially for actuator faults. However, SMC may suffer from chattering in control input. This has been addressed by variations of SMCs like boundary-layer SMC [18, 19], fuzzy SMC [20], and higher-order SMC [21].

Most variations of SMC are designed based on asymptotic stability without a guarantee for finite convergence time. One variation of SMC that can address this challenge is Terminal SMC (TSMC). One of the pioneering works in TSMC is [22], further expanded to multi-input and multi-output linear systems in [23], and nonlinear systems in [24]. A recent survey of the TSMC theory, its applications, key technical issues, and future challenges can be found in [25]. Recent examples of TSMC applications include the following. In [26], an adaptive TSMC strategy is proposed for buck converters. In [27], a TSMC formulation for finite-time position and attitude tracking of a quadrotor is presented. In [28], an adaptive nonsingular fast TSMC for tracking uncertain dynamical systems is developed. In [29] a TSMC scheme for robotic manipulators that combines fast convergence, chattering avoidance, and adaptive estimation of uncertainties is proposed.

Although early TSMC methods guaranteed finite-time convergence, their convergence time heavily relied on the initial conditions. The farther the initial conditions are from the desired states, the longer the convergence time is [25, 30, 31]. With the emergence of performance prescription control techniques, new TSMC designs achieved fixed-time convergence irrespective of the initial conditions [32]. Most fixed-time control methods suffer from singularity issues which can be partially alleviated using discontinuous control laws. For example, in [33], the singularity of TSMC is explained, and a new sliding surface is proposed to address it, followed by simulation-based verification on the inverted pendulum system. Similar strategies are used in [34] for chaos suppression in power systems, in [35] for attitude stabilization of a spacecraft, in [36], for fixed-time trajectory tracking of robotic manipulators, in [37], for synchronization control of multiple robotic manipulators, and in [38], for constrained fractional-order nonlinear systems. However, most existing methods rely on using the sign function in the control law which leads to chattering. Replacing the sign function with saturation or hyperbolic tangent can resolve the chattering issue, but leads to a slower convergence rate. A faster chattering-free controller is developed in [39]; however, as it will be shown in our numerical simulations, this controller has a steady-state error in the presence of sensor faults. We will build upon [39] to develop a controller with similar fast

convergence characteristics but superior fault tolerance.

Overall, the objective of the present paper is to develop a fast and fixed-time sensor fault detection and compensation technique for robotic manipulators. Inspired by [8], we will represent sensor faults as virtual actuator faults. Then, we will design an adaptive observer to detect faults and estimate the actual system states. The prominent feature of this observer is that it can guarantee the ultimate boundedness of state estimation error without the need to impose known bounds on the fault and/or its rate of change. Furthermore, we will develop a new chattering-free fixed-time TSMC control law. The control law lends well to the performance prescription control concept and enables imposing a boundary for the transient response of the system. We will integrate this control law with the aforementioned fault estimation observer and show system stability using Lyapunov stability analysis.

The main contributions of this paper include:

1. Designing a new fixed time controller capable of handling sensor fault while enabling performance prescription.
2. Developing a faster fixed-time control method inspired by [39] with a new second-order integral sliding surface. The controller offers the fast convergence property of the proposed sliding surface [39] while eliminating the steady-state error caused by perturbations, a feature that is lacking from the method in [39].
3. Building an adaptive observer to recover the healthy state variables from faulty measurement. The observer features a new adaptive term that makes it capable of performance guarantee without the need for the knowledge of the fault derivative.
4. Introducing two new adaptation laws by using auxiliary variables. One allows the estimation of unknown sensor fault; while the other enables the estimation of the sensor fault derivative bound.
5. The use of performance prescription concept to ensure errors remain in predetermined bound.

Notation. Throughout the paper, vectors, and matrices, if not explicitly stated, are assumed to have appropriate dimensions. For a given matrix A , $\lambda_{max}(A)$ and $\lambda_{min}(A)$ indicate the largest and smallest eigenvalues of A . $O_{n \times m}$ denote $n \times m$ zero matrix and I_n denotes the identity matrix. $\|\cdot\|$ denotes the 2-norm of a vector, and L_∞ represents the set of vectors with bounded ∞ -norm.

2. Problem Overview

Let us consider the dynamics of an n -link robotic manipulator described as follows

$$M(q)\ddot{q} + D(q, \dot{q})\dot{q} + G(q) = \tau, \quad (1)$$

where $q \in \mathbb{R}^n$ is the joints angular position, $\tau \in \mathbb{R}^n$ is the vector of torques applied to each joint, $M(q) \in \mathbb{R}^{n \times n}$ is the inertia matrix, $D(q, \dot{q}) \in \mathbb{R}^{n \times n}$ is the Centrifugal and Coriolis terms matrix, and $G(q) \in \mathbb{R}^n$ is the gravity vector. Equation (1) can be written in the following nonlinear form

$$\dot{x} = Ax + H(x, u), \quad y = Cx, \quad (2)$$

where $x = (x_1, x_2)^T$ with $x_1 = q$, $x_2 = \dot{q}$, $u = \tau$, $y = x_1$,

$$\begin{aligned} A &= \begin{pmatrix} O_{n \times n} & I_n \\ O_{n \times n} & O_{n \times n} \end{pmatrix}, \\ H(x, u) &= \begin{pmatrix} O_{n \times 1} \\ M^{-1}(x)(u - D(x)x_2 - G(x)) \end{pmatrix}, \text{ and} \\ C &= (I_n, O_{n \times n}). \end{aligned} \quad (3)$$

We assume that $H(x, u)$ is a Lipschitz function in x such that

$$\|H(x, u) - H(\hat{x}, u)\| \leq \kappa \|x - \hat{x}\|, \quad (4)$$

where $\kappa > 0$. This is a common assumption that has been used in observer design for robotic manipulators. Examples include [7, 40, 41]. To verify the validity of the above inequality, one needs to calculate the Jacobian of $H(x, u)$, and κ can be calculated as the supremum of the Jacobian over the domain of interest, as explained in [42].

When a sensor fault occurs, the measurement is represented by

$$y_f(t) = y(t) + Ef(t), \quad (5)$$

where y_f is the faulty measurement, and $f \in \mathbb{R}^m$ is the fault value, allowed to be time-varying. Note that we drop the time argument to simplify the mathematical notations. $E \in \mathbb{R}^{n \times m}$ is a constant matrix representing the propagation of fault in the output variable. We assume that f satisfies the following inequalities

$$\|f\|^2 \leq F \quad \text{and} \quad \|\dot{f}\|^2 \leq F_d, \quad (6)$$

where F and F_d are two unknown positive constants. It is noteworthy that the above assumptions are common. Examples of methods that assume an upper bound on \dot{f} include [43] and [44].

In this paper, we focus on both fault estimation and compensation. For fault estimation, our objective is to design an observer that can estimate fault and also recover y from faulty measurements y_f . Since we assume F and F_d are unknown, we will use an adaptive observer to achieve the above objective. For fault compensation, our objective is to design a fast fixed-time TSMC law that allows performance prescription on the trajectory tracking error. This control law must use the estimated states from the observer and must guarantee the system's stability. Figure 1 illustrates an overview of the system architecture. In the next two sections, we will explain the details of our observer and controller design.

3. Observer Design

To design the observer, we first represent the sensor faults as virtual actuator faults. As mentioned in Section 1, this representation is inspired by [8], and facilitates handling sensor faults.

The sensor fault can be represented as follows,

$$\dot{x}_v = -A_v x_v + A_v y_f, \quad (7)$$

where $x_v \in \mathbb{R}^n$ is the virtual actuator state vector, and $-A_v \in \mathbb{R}^{n \times n}$ is a constant Hurwitz matrix.

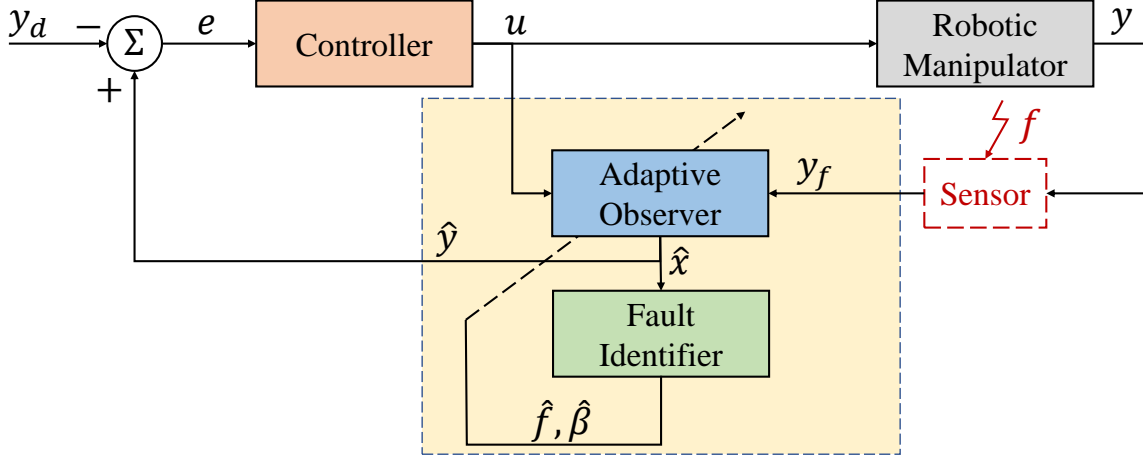


Figure 1: Block diagram of the proposed fault estimation and compensation method

Having defined sensor fault as a virtual actuator fault, an augmented system can be formed using (3) and (7) such that $x_a = (x, x_v)^T$ is the state vector of the augmented system with the following dynamics

$$\dot{x}_a = A_a x_a + H_a(x_a, u) + E_a f, \quad y_a = C_a x_a = x_v, \quad (8)$$

where

$$\begin{aligned} A_a &= \begin{pmatrix} A & O_{2n \times n} \\ A_v C & -A_v \end{pmatrix}, \\ H_a(x_a, u) &= \begin{pmatrix} H(x, u) \\ O_{n \times 1} \end{pmatrix}, \\ E_a &= \begin{pmatrix} O_{2n \times m} \\ A_v E \end{pmatrix}, \text{ and} \\ C_a &= \begin{pmatrix} O_{n \times 2n} & I_n \end{pmatrix}. \end{aligned} \quad (9)$$

Note that A_v must be chosen such that the pair (A_a, C_a) is observable.

To design the observer, we use \hat{x}_a to denote the estimation of x_a . Then, the estimated output will be $\hat{y}_a = C_a \hat{x}_a = \hat{x}_v$. We also use the notations $\tilde{x}_a = x_a - \hat{x}_a$ and $\tilde{y}_a = y_a - \hat{y}_a$ to indicate the estimation errors. We propose the following observer

$$\dot{\hat{x}}_a = A_a \hat{x}_a + H_a(\hat{x}_a, u) + E_a \hat{f}(t) + L \tilde{y} + \Lambda v, \quad (10)$$

where $L \in R^{3n \times n}$ and $\Lambda \in R^{3n \times n}$ are design parameters, \hat{f} is the estimation of fault, and $v \in R^n$ is a term that will be introduced shortly.

Let us first explain how \hat{f} is computed. We represent the sensor fault as

$$f(t) = \gamma d(t), \quad (11)$$

where $d \in \mathbb{R}^m$, and γ is a constant positive definite matrix in $\mathbb{R}^{m \times m}$. Therefore, $\hat{f} = \gamma \hat{d}$, and the problem of estimating \hat{f} is equivalent to estimating \hat{d} .

Remark 1: Note that γ serves as a scaling factor that adds an extra degree of freedom to tune the convergence rate of the fault estimator. While γ can be simply set to the identity matrix in many cases, our experiences with observer design reveal that this additional degree of freedom is generally useful in system tuning.

We use the following expressions to estimate d .

$$\hat{d} = \hat{\pi} + \Gamma E^T \hat{y}_a, \quad (12)$$

where $\hat{\pi}$ is an adaptive term with the following dynamics

$$\dot{\hat{\pi}} = -\Gamma E^T C_a \left(A_a \hat{x}_a + H_a(\hat{x}_a, u) + E_a \hat{f} \right), \quad (13)$$

where $\Gamma \in \mathbb{R}^{m \times m}$ is a positive-definite design parameter. As it will be revealed in our Lyapunov analysis, $\hat{\pi}$ can be regarded as the estimate of the value represented by

$$\pi = d - \Gamma E^T y_a. \quad (14)$$

The adaptation law (13) helps the observer to deal with the unknown upper bound of f i.e. F .

As we deal with the challenging case in which the upper bound of \dot{f} , i.e. F_d , is unknown too, we introduce the following expression for v

$$v = \Upsilon \tilde{y} + \hat{\beta} \tilde{y} \|\tilde{y}\|^{-2} \tanh^2(\rho_1^{-1} \|\tilde{y}\|^2), \quad (15)$$

where $\Upsilon \in \mathbb{R}^{n \times n}$ and is positive-definite, and $\rho_1 > 0$. Similar to $\hat{\pi}$, $\hat{\beta}$ is an adaptive parameter but with the following adaptation law

$$\dot{\hat{\beta}} = 2 \tanh^2(\rho_1^{-1} \|\tilde{y}\|^2) - \rho_2 \hat{\beta}, \quad (16)$$

where $\rho_2 > 0$. Again, as it will be revealed in our Lyapunov analysis, $\hat{\beta}$ is an estimate of a parameter defined as

$$\beta = 0.5 \lambda_{\min}^{-1}(\gamma) \lambda_{\max} \left((\Gamma^{-1})^T \Gamma^{-1} \right) F_d. \quad (17)$$

Therefore, by using (16), the observer can deal with unknown F_d .

Remark 2: As it will become clear shortly, the reason to use $\tanh^2(\cdot)$ is the desirable properties of this function in the vicinity of the origin. Our stability analysis below will lead to the evaluation of terms in the form of $1 - 2 \tanh^2(\cdot)$ where we can apply Lemma 3 (given in Appendix A) to establish stability criteria for design parameters while ensuring the smoothness of parameters evolution with time.

To determine the stability criteria for the design parameters, let us first write the estimation error dynamics using (8), (10), and $\tilde{x}_a = x_a - \hat{x}_a$.

$$\dot{\tilde{x}}_a = (A_a - LC_a) \tilde{x}_a + E_a \tilde{f} + H_a(x_a, u) - H_a(\hat{x}_a, u) - \Lambda v, \quad (18)$$

where $\tilde{f} = f - \hat{f}$ is the fault estimation error. Using (11), (12), and (14), we have

$$\tilde{f} = \gamma (\tilde{\pi} + \Gamma E^T C_a \tilde{x}_a), \quad (19)$$

where $\tilde{\pi} = \pi - \hat{\pi}$. Let us define the following Lyapunov function

$$V_1 = \tilde{x}_a^T P \tilde{x}_a + 0.5 \tilde{\pi}^T \Gamma^{-1} \tilde{\pi} + 0.5 \tilde{\beta}^2, \quad (20)$$

where $P > 0$, and $\tilde{\beta} = \beta - \hat{\beta}$. Taking the time derivative of V_1 and substituting (18) yields

$$\begin{aligned} \dot{V}_1 &= \tilde{x}_a^T P \dot{\tilde{x}}_a + \dot{\tilde{x}}_a^T P \tilde{x}_a + \tilde{\pi}^T \Gamma^{-1} \dot{\tilde{\pi}} + \tilde{\beta} \dot{\tilde{\beta}} \\ &= \tilde{x}_a^T \left(P(A_a - LC_a) + (A_a - LC_a)^T P \right) \tilde{x}_a + \tilde{x}_a^T P E_a \tilde{f} + \tilde{f}^T E_a^T P \tilde{x}_a \\ &\quad + \tilde{x}_a^T P (H_a(x_a, u) - H_a(\hat{x}_a, u)) + (H_a(x_a, u) - H_a(\hat{x}_a, u))^T P \tilde{x}_a \\ &\quad - \tilde{x}_a^T P \Lambda v - v^T \Lambda^T P \tilde{x}_a + \tilde{\pi}^T \Gamma^{-1} \dot{\tilde{\pi}} + \tilde{\beta} \dot{\tilde{\beta}}, \end{aligned} \quad (21)$$

In the following, we intend to find upper bounds on some of the terms on the right-hand side of (21). Our developments rely on the application of Young's inequality given in Appendix A.

For the second and third terms in the right-hand side of (21), we apply (86) to write

$$\tilde{x}_a^T P E_a \tilde{f} + \tilde{f}^T E_a^T P \tilde{x}_a \leq \frac{2}{3} \tilde{x}_a^T P P^T \tilde{x}_a + 3 \tilde{x}_a^T \varepsilon_1 \varepsilon_1^T \tilde{x}_a + 3 \tilde{\pi}^T \varepsilon_2 \varepsilon_2^T \tilde{\pi}, \quad (22)$$

where $\varepsilon_1 = C_a^T E \Gamma^T \gamma^T E_a^T$ and $\varepsilon_2 = \gamma^T E_a^T$. For the fourth term, we apply (86) and use the Lipschitz assumption (4) to write

$$\begin{aligned} (H_a(x_a, u) - H_a(\hat{x}_a, u))^T P \tilde{x}_a + \tilde{x}_a^T P (H_a(x_a, u) - H_a(\hat{x}_a, u)) \\ \leq \frac{1}{3} \tilde{x}_a^T P P^T \tilde{x}_a + 3 \kappa^2 \tilde{x}_a^T \tilde{x}_a. \end{aligned} \quad (23)$$

For $\dot{\tilde{\pi}}$, we use (8), (13), (14), and $\tilde{\pi} = \pi - \hat{\pi}$ to write

$$\dot{\tilde{\pi}} = \dot{d} - \Gamma E^T C_a (A_a \tilde{x}_a + E_a \tilde{f}) - \Gamma E^T C_a (H_a(x_a, u) - H_a(\hat{x}_a, u)). \quad (24)$$

Therefore, $\tilde{\pi}^T \Gamma^{-1} \dot{\tilde{\pi}}$ in (21) becomes

$$\begin{aligned} \tilde{\pi}^T \Gamma^{-1} \dot{\tilde{\pi}} &= \tilde{\pi}^T \Gamma^{-1} \dot{d} - \tilde{\pi}^T E^T C_a A_a \tilde{x}_a - \tilde{\pi}^T E^T C_a E_a \tilde{f} \\ &\quad - \tilde{\pi}^T E^T C_a (H_a(x_a, u) - H_a(\hat{x}_a, u)). \end{aligned} \quad (25)$$

Again, by applying Young's inequality (86) we can derive upper bounds for each term on the right-hand side of (25). To this end, the first term leads to

$$\tilde{\pi}^T \Gamma^{-1} \dot{d} \leq \frac{1}{2} \tilde{\pi}^T \tilde{\pi} + \frac{1}{2} \dot{d}^T (\Gamma^{-1})^T \Gamma^{-1} \dot{d} \leq \frac{1}{2} \tilde{\pi}^T \tilde{\pi} + \beta, \quad (26)$$

where β was defined in (17). Similarly, we have

$$-\tilde{\pi}^T E^T C_a A_a \tilde{x}_a \leq \frac{1}{2c_1} \tilde{\pi}^T \varepsilon_3 \varepsilon_3^T \tilde{\pi} + \frac{c_1}{2} \tilde{x}_a^T \tilde{x}_a, \quad (27)$$

where $\varepsilon_3 = E^T C_a A_a$, and c_1 is an arbitrary positive constant. We can also write

$$-\tilde{\pi}^T E^T C_a E_a \gamma \Gamma E^T C_a \tilde{x}_a \leq \frac{1}{2c_2} \tilde{\pi}^T \varepsilon_4 \varepsilon_4^T \tilde{\pi} + \frac{c_2}{2} \tilde{x}_a^T \tilde{x}_a, \quad (28)$$

where $\varepsilon_4 = E^T C_a E_a \gamma \Gamma E^T C_a$ and c_2 is an arbitrary positive constant. Next, we have

$$-\tilde{\pi}^T E^T C_a (H_a(x_a, u) - H_a(\hat{x}_a, u)) \leq \kappa^2 \tilde{x}_a^T \tilde{x}_a + \frac{1}{4} \tilde{\pi}^T \varepsilon_5 \varepsilon_5^T \tilde{\pi}, \quad (29)$$

where $\varepsilon_5 = E^T C_a$. Substituting the expressions from (22) to (29) in (21) leads to

$$\dot{V}_1 \leq -\tilde{x}_a^T Q_1 \tilde{x}_a - \tilde{\pi}^T Q_2 \tilde{\pi} - \tilde{x}_a^T P \Lambda v - v^T \Lambda^T P \tilde{x}_a + \beta + \tilde{\beta} \dot{\tilde{\beta}}, \quad (30)$$

where

$$Q_1 = - \left((A_a - LC_a)^T P + P (A_a - LC_a) + P^2 + 4\kappa^2 I_{3n} + 3\varepsilon_1 \varepsilon_1^T + \frac{c_1}{2} + \frac{c_2}{2} \right), \quad (31)$$

and

$$Q_2 = - \left(-E^T C_a E_a + 3\varepsilon_2 \varepsilon_2^T + \frac{1}{2} + \frac{1}{2c_1} \varepsilon_3 \varepsilon_3^T + \frac{1}{2c_2} \varepsilon_4 \varepsilon_4^T + \frac{1}{4} \varepsilon_5 \varepsilon_5^T \right). \quad (32)$$

Now, let us choose

$$\Lambda = P^{-1}C_a^T. \quad (33)$$

It follows from $\tilde{y} = C_a \tilde{x}_a$ that

$$-\tilde{x}_a^T P \Lambda v - v^T \Lambda^T P \tilde{x}_a = -2\tilde{x}_a^T P \Lambda v = -2\tilde{y}^T v. \quad (34)$$

Substituting (34) in (30), adding and subtracting $2\beta \tanh^2(\rho_1^{-1} \|\tilde{y}\|^2)$, and using $\tilde{\beta} = \beta - \hat{\beta} \rightarrow \dot{\tilde{\beta}} = -\dot{\hat{\beta}}$ yields

$$\begin{aligned} \dot{V}_1 \leq & -\tilde{x}_a^T Q_1 \tilde{x}_a - \tilde{\pi}^T Q_2 \tilde{\pi} - 2\tilde{y}^T \Upsilon \tilde{y} + \tilde{\beta} \left(2\tanh^2(\rho_1^{-1} \|\tilde{y}\|^2) - \dot{\tilde{\beta}} \right) \\ & + \beta \left(1 - 2\tanh^2(\rho_1^{-1} \|\tilde{y}\|^2) \right). \end{aligned} \quad (35)$$

For the fourth term in the right-hand side of (35), we can use (16) and Young's inequality (86) to write

$$\begin{aligned} \tilde{\beta} \left(2\tanh^2(\rho_1^{-1} \|\tilde{y}\|^2) - \dot{\tilde{\beta}} \right) &= \rho_2 \tilde{\beta} \hat{\beta} = \rho_2 \tilde{\beta} (\beta - \tilde{\beta}) \\ &\leq -0.5 \left(\rho_2 \tilde{\beta}^2 - \rho_2 \beta^2 \right). \end{aligned} \quad (36)$$

Therefore,

$$\dot{V}_1 \leq -\tilde{x}_a^T Q_1 \tilde{x}_a - \tilde{\pi}^T Q_2 \tilde{\pi} + 0.5\rho\beta^2 - 0.5\rho\tilde{\beta}^2 + \beta \left(1 - 2\tanh^2(\rho_1^{-1} \|\tilde{y}\|^2) \right), \quad (37)$$

which can be re-written in the form of

$$\dot{V}_1 \leq -\alpha V_1 + \delta \quad (38)$$

where $\alpha = \left\{ \frac{\lambda_{\min}(Q_1)}{\lambda_{\max}(P)}, \frac{2\lambda_{\min}(Q_2)}{\lambda_{\max}(\Gamma^{-1})}, \rho \right\}$, and

$$\delta = \begin{cases} 0.5\rho_2\beta^2, & \text{if } \|\tilde{y}\| \geq 0.8814\rho_1, \\ 0.5\rho_2\beta^2 + \beta, & \text{if } \|\tilde{y}\| < 0.8814\rho_1. \end{cases} \quad (39)$$

If $Q_1 > 0$, $Q_2 > 0$, and $\rho_2 > 0$, then from Lemma 4 (given in Appendix A) we have

$$V_1(t) \leq V_1(0)e^{-\alpha t} + \int_0^t e^{-\alpha(t-\tau)} \delta(\tau) d\tau. \quad (40)$$

In other words,

$$V_1(t) \leq \left(V_1(0) - \frac{\delta}{\alpha} \right) e^{-\alpha t} + \frac{\delta}{\alpha}. \quad (41)$$

It follows from the definition of V_1 (20) that

$$\|\tilde{x}_a\| \leq \sqrt{\frac{\max(V_1(0), \frac{\delta}{\alpha})}{\lambda_{\min}(P)}}. \quad (42)$$

Therefore, the estimation error will remain in an adjustable neighborhood of the origin, and this guarantees that with the appropriate choice of design parameters, \hat{x}_a can become close to x_a .

Remark 3: The key feature of the proposed observer (10) is the adaptation laws (13) and (16) that are designed in a way that can estimate f without the need to know F and F_d . The two adaptation laws also provide a higher degree of freedom in tuning the system which can lead to improved estimation performance.

4. Controller Design

This section presents the controller design. As mentioned in Section 1, our objective is to design a fault-tolerant controller that can integrate well with the fault detection observer, and establish a performance-prescribed, fast, and fixed-time convergence.

Let us first decompose L and Λ as $L = (L_1, L_2, L_3)^T$ and $\Lambda = (\Lambda_1, \Lambda_2, \Lambda_3)^T$. Based on the observer (10), we have

$$\begin{cases} \dot{\hat{x}}_1 = \hat{x}_2 + L_1 \tilde{y} + \Lambda_1 v \\ \dot{\hat{x}}_2 = M^{-1}(\hat{x}_1)(u - D(\hat{x}_1, \hat{x}_2)\hat{x}_2 - G(\hat{x}_1)) + L_2 \tilde{y} + \Lambda_2 v \end{cases} \quad (43)$$

Let y_d be the desired trajectory, and $e = \hat{x}_1 - y_d$ be the tracking error. Then, the error dynamics takes the following form

$$\begin{cases} \dot{e} = \hat{x}_2 + L_1 \tilde{y} + \Lambda_1 v - \dot{y}_d \\ \ddot{e} = M^{-1}(\hat{x}_1)(u - D(\hat{x}_1, \hat{x}_2)\hat{x}_2 - G(\hat{x}_1)) + L_2 \tilde{y} + L_1 \dot{\tilde{y}} + \Lambda_2 v + \Lambda_1 \dot{v} - \ddot{y}_d \end{cases} \quad (44)$$

Using (7), (10), and (15), we have

$$\dot{y} = \dot{x}_v = -A_v x_v + A_v y_f, \quad (45)$$

$$\dot{\hat{y}} = \dot{\hat{x}}_v = (A_v C - A_v) \hat{x} + A_v E \hat{f} + L_3 \tilde{y} + \Lambda_3 v, \quad (46)$$

and

$$\dot{v} = \Upsilon \dot{\hat{y}} + \hat{\beta} \tilde{y} \|\tilde{y}\|^{-2} \tanh^2(\rho_1^{-1} \|\tilde{y}\|^2) + \hat{\beta} \dot{\tilde{y}} \|\tilde{y}\|^{-2} \tanh^2(\rho_1^{-1} \|\tilde{y}\|^2) + \hat{\beta} \tilde{y} \Psi, \quad (47)$$

where

$$\Psi = \|\tilde{y}\|^{-4} (\Theta_1 - \Theta_2), \quad (48)$$

$$\Theta_1 = 2\rho_1^{-1} \|\tilde{y}\|^2 \tanh(\rho_1^{-1} \|\tilde{y}\|^2) (1 - \tanh^2(\rho_1^{-1} \|\tilde{y}\|^2)) (\dot{\tilde{y}}^T \tilde{y} + \tilde{y}^T \dot{\tilde{y}}), \quad (49)$$

and

$$\Theta_2 = \tanh^2(\rho_1^{-1} \|\tilde{y}\|^2) (\dot{\tilde{y}}^T \tilde{y} + \tilde{y}^T \dot{\tilde{y}}). \quad (50)$$

4.1. Performance Prescription

To enable performance prescription, let us define a prescribed performance function $\mu(t)$ as follows

$$\mu(t) = (\mu_0 - \mu_\infty) e^{-lt} + \mu_\infty, \quad (51)$$

where $\mu_0 > e(0)$, and $\mu_\infty > 0$, and $l > 0$. Note that $\mu(t)$ is a positive and descending function. If we find a way to ensure the following criteria

$$-\mu(t) \leq e(t) \leq \mu(t), \quad (52)$$

then we can shape the tracking error trajectory using the definition of $\mu(t)$. As such, the inequality (52) is our performance prescription control objective.

To facilitate dealing with the inequality (52), we define a new variable as follows

$$z(t) = T^{-1}(\omega) \quad (53)$$

where $\omega = \frac{e(t)}{\mu(t)}$, and $T(z(t))$ is a strictly monotonic ascending function with the following properties:

$$T(0) = 0, \lim_{z \rightarrow +\infty} T(z) = +1, \lim_{z \rightarrow -\infty} T(z) = -1, \text{ and } \forall z \in L_\infty \rightarrow \|T(z)\| < 1. \quad (54)$$

Let \underline{z} and \bar{z} be the lower and upper bounds on z . Since T is a strictly uniform ascending function and $\mu(t)$ is always positive, we can write

$$\mu(t) T(\underline{z}) \leq \mu(t) T(z(t)) \leq \mu(t) T(\bar{z}). \quad (55)$$

According to (53), $e(t) = \mu(t) T(z(t))$. Therefore, (52) can be fulfilled by ensuring z is bounded. This implies that our performance prescription objective is to find an appropriate mapping T and a control law that guarantees the boundness of z .

A suitable choice for the function T is $\tanh(\cdot)$. Using its inverse, we have

$$z = T^{-1}(\omega) = 0.5 \ln \left(\frac{1 + \omega}{1 - \omega} \right). \quad (56)$$

As such, we will use (56) in designing our TSMC control law.

4.2. Terminal Sliding Mode Dynamics

Our TSMC developments here are inspired by [39]. The TSMC approach presented in [39] has the advantage of fast fixed-time convergence; however, as it will be shown in our numerical simulations, it suffers from steady-state error in the presence of sensor fault. To address this, we propose a new integral second-order sliding surface, as opposed to the first-order sliding surface developed in [39].

Remark 4: *As it will be shown in our theoretical developments and numerical simulations, using the new integral second-order sliding surface reduces the steady-state error while maintaining similar fast convergence characteristics of its first-order counterpart in [39].*

Remark 5: *Note that we will base our developments on z instead of e to enable performance prescription. This is another key difference of our work compared to [39].*

Let us define the following sliding surface

$$\sigma = \dot{\eta} + \bar{g}(\eta), \quad (57)$$

where

$$\eta = z + \int_0^t \bar{g}(z(\tau)) d\tau. \quad (58)$$

In this definition, $g(\cdot)$ is a scalar function defined as follows

$$g(\chi) = \frac{1}{\varphi(\chi)} \left(\underline{\lambda} \operatorname{sgn}(\chi) |\chi|^{p^*} + \bar{\lambda} \operatorname{sgn}(\chi) |\chi|^{\frac{\bar{p}}{q}} \right), \quad (59)$$

where χ is an arbitrary scalar serving as the argument for g , and

$$p^* = \frac{1}{2} + \frac{p}{2\underline{q}} + \left(\frac{p}{2\underline{q}} - \frac{1}{2} \right) \operatorname{sgn}(|\chi| - 1), \quad (60)$$

$$\varphi(\chi) = a + (1 - a) e^{-b|\chi|^c}, \quad (61)$$

$\underline{\lambda}$, $\bar{\lambda}$, $a < 1$, and b are positive constants, c is an even positive integer, \underline{p} , \underline{q} , \bar{p} , and \bar{q} are positive odd integers such that $\underline{p} > \underline{q}$ and $\bar{p} < \bar{q}$. To construct the sliding surface, we define two vectors as $\bar{g}(z) = (g(z_1), g(z_2), \dots, g(z_n))^T$ and $\bar{g}(\eta) = (g(\eta_1), g(\eta_2), \dots, g(\eta_n))^T$.

As it will be revealed in our Lyapunov analysis shortly, the use of (57) will lead to the following terminal sliding dynamics

$$\begin{cases} \chi_2 = \chi_1 + \int_0^t \frac{1}{\varphi(\chi_1(\tau))} (\underline{\lambda} \operatorname{sgn}(\chi_1(\tau)) |\chi_1(\tau)|^{p^*} + \bar{\lambda} \operatorname{sgn}(\chi_1(\tau)) |\chi_1(\tau)|^{\frac{\bar{p}}{\bar{q}}}) d\tau, \\ \dot{\chi}_2 = -\frac{1}{\varphi(\chi_2)} (\underline{\lambda} \operatorname{sgn}(\chi_2) |\chi_2|^{p^*} + \bar{\lambda} \operatorname{sgn}(\chi_2) |\chi_2|^{\frac{\bar{p}}{\bar{q}}}), \end{cases} \quad (62)$$

where $\chi_1 = z_i$ and $\chi_2 = \eta_i$ for $i = 1, \dots, n$. We will establish our convergence results based on findings in [39] which is summarized as Lemma 6 in Appendix A of this paper.

First, let us take the derivative of the first equation in (62). We have

$$\dot{\chi}_2 = \dot{\chi}_1 + \frac{1}{\varphi(\chi_1)} (\underline{\lambda} \operatorname{sgn}(\chi_1) |\chi_1|^{p^*} + \bar{\lambda} \operatorname{sgn}(\chi_1) |\chi_1|^{\frac{\bar{p}}{\bar{q}}}). \quad (63)$$

According to Lemma 6 and the second equation of (62), χ_2 will converge to the origin in fixed time. When $\chi_2 = 0$ and $\dot{\chi}_2 = 0$, (63) becomes

$$\dot{\chi}_1 = -\frac{1}{\varphi(\chi_1)} (\underline{\lambda} \operatorname{sgn}(\chi_1) |\chi_1|^{p^*} + \bar{\lambda} \operatorname{sgn}(\chi_1) |\chi_1|^{\frac{\bar{p}}{\bar{q}}}). \quad (64)$$

Again, based on Lemma 6, we infer that χ_1 will converge to the origin in fixed time.

Note that in the definition of the function g and its design parameters, we follow the criteria given by Lemma 6. Since $\dot{\chi}_1$ and $\dot{\chi}_2$ have the same dynamics as in (96), the convergence time for them will be in the form of (97), which is identical to [39].

4.3. Control Law and Stability Analysis

This section presents our fault-tolerant control law based on the sliding surface (57).

Similar to most sliding mode control designs, let us consider the Lyapunov function

$$V_2 = \frac{1}{2} \sigma^T \sigma, \quad (65)$$

Taking the time-derivative of (65) yields $\dot{V}_2 = \sigma^T \dot{\sigma}$. In the following, we calculate $\dot{\sigma}$ and substitute in \dot{V}_2 .

Evaluating (57) leads to the following expression

$$\dot{\sigma} = \ddot{z} + \dot{\bar{g}}(z) + \dot{\bar{g}}(\eta). \quad (66)$$

For the first term in the right-hand side of (66), we take the derivative of (56). It follows that

$$\dot{z} = \frac{\partial T^{-1}}{\partial \omega} \dot{\omega} = r(\dot{e} - se), \quad (67)$$

where

$$r = \operatorname{diag} \left((\mu(1 - \omega_1^2))^{-1}, \dots, (\mu(1 - \omega_n^2))^{-1} \right), \quad (68)$$

and $s = \dot{\mu} \mu^{-1} I_n$. Next,

$$\ddot{z} = \dot{r}(\dot{e} - se) + r(\ddot{e} - \dot{s}e - s\dot{e}), \quad (69)$$

where

$$\dot{s} = \text{diag} \left(\frac{\ddot{\mu} \mu - \dot{\mu}^2}{\mu^2}, \dots, \frac{\ddot{\mu} \mu - \dot{\mu}^2}{\mu^2} \right), \quad (70)$$

and

$$\dot{r} = \text{diag} \left(\frac{-\dot{\mu} (1 - \omega_1^2) + 2 \mu \omega_1 \dot{\omega}_1}{(\mu (1 - \omega_1^2))^2}, \dots, \frac{-\dot{\mu} (1 - \omega_n^2) + 2 \mu \omega_n \dot{\omega}_n}{(\mu (1 - \omega_n^2))^2} \right). \quad (71)$$

By defining $R = \dot{r}(\dot{e} - se) - r(\dot{s}e + s\dot{e})$, \ddot{z} can be written as

$$\ddot{z} = R + r\ddot{e}. \quad (72)$$

For the second and third terms in the right-hand side of (66), we take the derivative of (59). This leads to the following expression

$$\begin{aligned} \dot{g}(\chi) = & -\frac{\dot{\varphi}(\chi)}{\varphi^2(\chi)} \left(\underline{\lambda} \text{sgn}(\chi) |\chi|^{p^*} + \bar{\lambda} \text{sgn}(\chi) |\chi|^{\frac{\bar{p}}{q}} \right) \\ & + \frac{1}{\varphi(\chi)} \left(\underline{\lambda} p^* |\chi|^{p^*-1} + \bar{\lambda} \frac{\bar{p}}{q} |\chi|^{\frac{\bar{p}}{q}-1} \right) \dot{\chi}, \end{aligned} \quad (73)$$

where

$$\dot{\varphi}(\chi) = -(1-a) b c \text{sgn}(\chi) |\chi|^{c-1} \dot{\chi} e^{-b|\chi|^c}. \quad (74)$$

Substituting (72) and (73) into (66) yields

$$\dot{\sigma} = \ddot{z} + \dot{g}(z) + \dot{g}(\eta) = R + r\ddot{e} + \dot{g}(z) + \dot{g}(\eta). \quad (75)$$

Then, from (44) it follows that

$$\begin{aligned} \dot{\sigma} = & r M^{-1}(\hat{x}_1) (u - D(\hat{x}_1, \hat{x}_2) \hat{x}_2 - G(\hat{x}_1)) \\ & + M(\hat{x}_1) (L_2 \tilde{y} + L_1 \dot{\tilde{y}} + \Lambda_2 v + \Lambda_1 \dot{v} - \ddot{y}_d) \\ & + R + \dot{g}(z) + \dot{g}(\eta). \end{aligned} \quad (76)$$

Let us define the control law as follows

$$\begin{aligned} u = & D(\hat{x}_1, \hat{x}_2) \hat{x}_2 + G(\hat{x}_1) - M(\hat{x}_1) (L_2 \tilde{y} + L_1 \dot{\tilde{y}} + \Lambda_2 v + \Lambda_1 \dot{v} - \ddot{y}_d) \\ & - M(\hat{x}_1) r^{-1} (R + \dot{g}(z) + \dot{g}(\eta) + k_{1\sigma} \sigma + c_{1\sigma} \sigma^{p_\sigma/q_\sigma} + \bar{c}_{1\sigma} \sigma^{\bar{p}_\sigma/\bar{q}_\sigma}), \end{aligned} \quad (77)$$

where $k_{1\sigma}$, $c_{1\sigma}$ and $\bar{c}_{1\sigma}$ are positive constants, and p_σ , q_σ , \bar{p}_σ and \bar{q}_σ are positive odd numbers such that $p_\sigma > q_\sigma$ and $\bar{p}_\sigma < \bar{q}_\sigma$. Furthermore, $\sigma^{p_\sigma/q_\sigma} = (\sigma_1^{p_\sigma/q_\sigma}, \dots, \sigma_n^{p_\sigma/q_\sigma})^T$ and $\sigma^{\bar{p}_\sigma/\bar{q}_\sigma} = (\sigma_1^{\bar{p}_\sigma/\bar{q}_\sigma}, \dots, \sigma_n^{\bar{p}_\sigma/\bar{q}_\sigma})^T$.

Substituting (77) in (76) and using $\dot{V}_2 = \sigma^T \dot{\sigma}$ yields

$$\dot{V}_2 = -k_{1\sigma} \sigma^T \sigma - c_{1\sigma} \sigma^T \sigma^{p_\sigma/q_\sigma} - \bar{c}_{1\sigma} \sigma^T \sigma^{\bar{p}_\sigma/\bar{q}_\sigma}, \quad (78)$$

where

$$\sigma^T \sigma^{p_\sigma/q_\sigma} = \sigma_1^{1+p_\sigma/q_\sigma} + \dots + \sigma_n^{1+p_\sigma/q_\sigma}, \quad (79)$$

and

$$\sigma^T \sigma^{\bar{p}_\sigma/\bar{q}_\sigma} = \sigma_1^{1+\bar{p}_\sigma/\bar{q}_\sigma} + \dots + \sigma_n^{1+\bar{p}_\sigma/\bar{q}_\sigma}. \quad (80)$$

Based on the definition of V_2 in (65), (87) and (88), we have

$$\alpha_\sigma V_2^{\beta_v} \leq \sigma^T \sigma^{p_\sigma/q_\sigma} \quad (81)$$

where $\beta_v = (p_\sigma + q_\sigma)/2q_\sigma$, $\alpha_\sigma = 2^{(p_\sigma+q_\sigma)/2q_\sigma} \eta^{(p_\sigma-q_\sigma)/2q_\sigma}$, and

$$\bar{\alpha}_\sigma V_2^{\bar{\beta}_v} \leq \sigma^T \sigma^{\bar{p}_\sigma/\bar{q}_\sigma}, \quad (82)$$

with $\bar{\beta}_v = \frac{(\bar{p}_\sigma + \bar{q}_\sigma)}{2\bar{q}_\sigma}$ and $\bar{\alpha}_\sigma = 2^{\frac{(\bar{p}_\sigma + \bar{q}_\sigma)}{2\bar{q}_\sigma}}$. Thus, \dot{V}_2 satisfies

$$\dot{V}_2 \leq -2k_{1\sigma} V_2 - c_{1\sigma} \alpha_\sigma V_2^{\beta_v} - \bar{c}_{1\sigma} \bar{\alpha}_\sigma V_2^{\bar{\beta}_v}. \quad (83)$$

Let $\alpha_\nu = c_{1\sigma} \alpha_\sigma$ and $\bar{\alpha}_\nu = \bar{c}_{1\sigma} \bar{\alpha}_\sigma$. Then, it follows that

$$\dot{V}_2 \leq -\alpha_\nu V_2^{\beta_v} - \bar{\alpha}_\nu V_2^{\bar{\beta}_v}, \quad (84)$$

which guarantees fixed-time stability of σ according to Lemma 5 (given in Appendix A). This implies that η and z are fixed-time stable.

Furthermore, based on (56), we infer that $e \rightarrow 0$ when $z \rightarrow 0$. Since $\tilde{x}_1 = x_1 - \hat{x}_1$, we can write $x_1 = \tilde{x}_1 + \hat{x}_1 = \tilde{x}_1 + e + y_d$. Since $e \rightarrow 0$ and \tilde{x}_1 is ultimately bounded, it can be inferred that x_1 converges to a neighborhood of y_d .

We can also show that x_2 converges to a neighborhood of \dot{y}_d . To this end, from (57) and (58), we note that $\sigma = \dot{z} + \bar{g}(z) + \bar{g}(\eta)$. Since $\bar{g}(0) = 0$, at the time that $\sigma \rightarrow 0$, we have $\dot{z} \rightarrow 0$. It follows from (67) that $\dot{e} \rightarrow e$. When $\sigma \rightarrow 0$, we have $e \rightarrow 0$. Therefore, $\dot{e} \rightarrow 0$.

With that in mind, we can now examine the first equation in (44) as follows. Since the observer guarantees the ultimate boundedness of estimation error, \tilde{y} is arbitrarily small. This implies that v is arbitrarily small as it is given by (15). We also established that $\dot{e} \rightarrow 0$ in the above paragraph. Putting all these together and evaluating the first equation in (44) implies that \hat{x}_2 will converge to a neighborhood of \dot{y}_d . Finally, we note that $x_2 = \tilde{x}_2 + \hat{x}_2$, and since \tilde{x}_2 is arbitrarily small, we can infer that x_2 will converge to a neighborhood of \dot{y}_d .

5. Numerical Simulations

This section presents numerical simulations to evaluate the effectiveness of the proposed method.

5.1. Example 1: Two-Link Rigid Robotic Manipulator

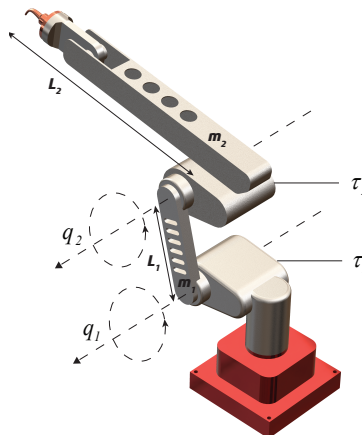


Figure 2: Two-link rigid robotics manipulator system

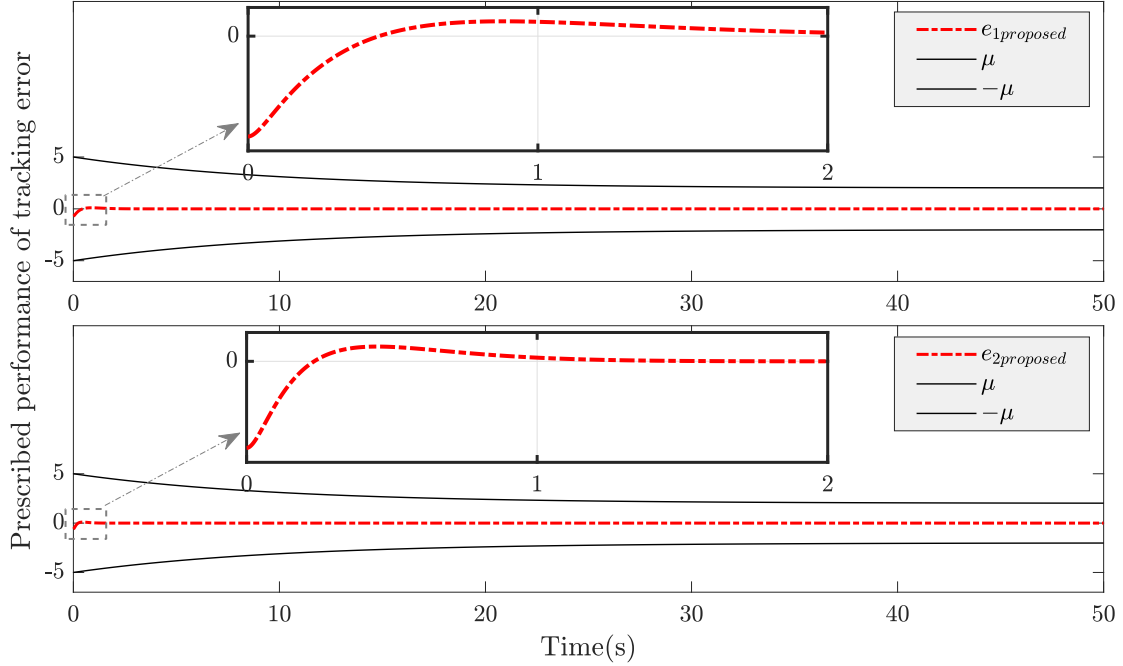


Figure 3: Tracking error within the bounds of the performance prescription function with $\mu_0 = 5$, $\mu_\infty = 2$, and $l = 0.1$.

In this example, we consider a two-link rigid robotic manipulator (Fig. 2), and compare our method with [39] and [7]. The parameters of the robot model are selected according to [39] to minimize confounding errors in comparisons.

Before the comparison, we would like to highlight the benefits of performance prescription. Figures 3 and 4 show the tracking error of the robot controlled by our method in nominal conditions. Two different performance prescription functions are considered, one with $\mu_0 = 5$, $\mu_\infty = 2$, and $l = 0.1$ (Fig. 3), and the other with $\mu_0 = 1$, $\mu_\infty = 0.01$ and $l = 10$ (Fig. 4). The rest of the design parameters are set according to B, and the robot joints are tasked to follow sinusoidal trajectories.

It is evident that in both cases the tracking error is bounded within the funnels set by the prescription functions. Clearly, setting tighter bounds in Fig. 4 has not violated the boundaries and the controller has managed to keep $\|e_i\| \leq 0.01$ with a fast decay rate. This shows the degree of flexibility that our method offers in prescribing the tracking error performance, a feature that is missing from the benchmark methods that will be discussed shortly and also from many other methods in fault-tolerant control literature.

Let us now compare our method with methods proposed in [39] and [7]. We set the design parameters for our controller as mentioned above. For the method by Gao et al., we used the same parameters that were proposed in [39]. For the method by Ma et al., there was a need to fine-tune the parameters. After several simulation trials, we chose the design parameters according to the original paper [7] with the exceptions of $G_1 = 8$ and $\theta = 12$. Furthermore, we set the initial conditions of all adaptation laws to zero. We tasked the robot joints to follow sinusoidal trajectories and considered the following fault on the first angular position sensor with $E = (1 \ 0)^T$, and

$$f = \begin{cases} 0, & t < 25 \\ 3 \tanh\left(\frac{(t-25)^2}{0.2}\right), & t \geq 25 \end{cases} \quad (85)$$

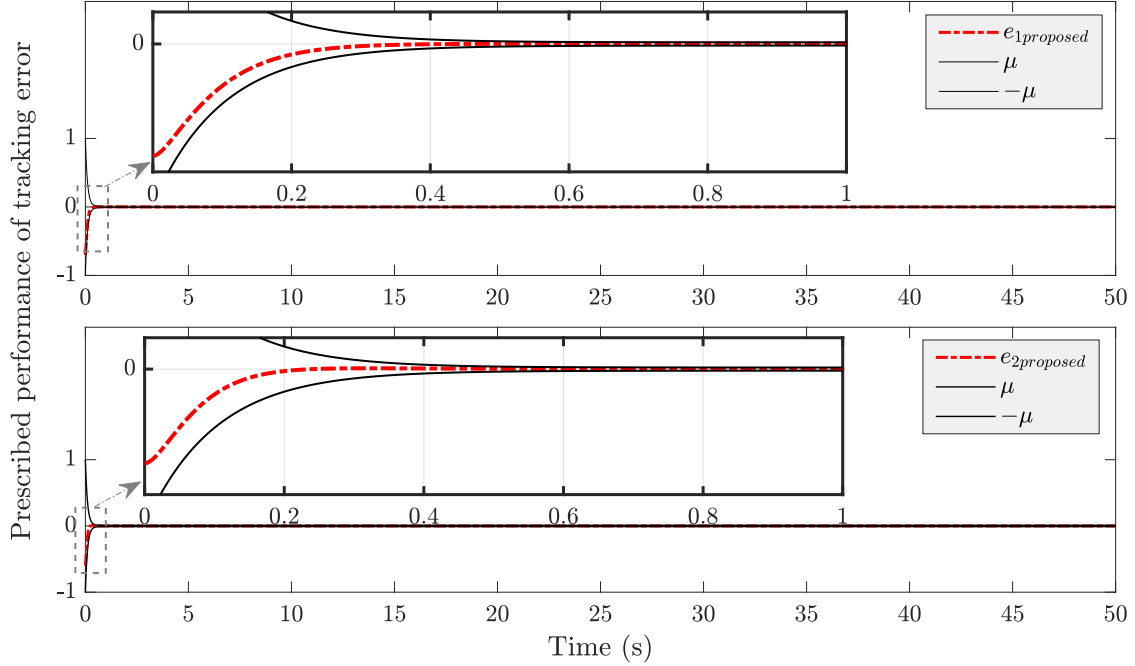


Figure 4: Tracking error within the bounds of the performance prescription function $\mu_0 = 1$, $\mu_\infty = 0.01$, and $l = 10$.

Figures 5 and 6 demonstrate the trajectory-tracking performance and control inputs of all three methods. When the sensor fault occurs at $t = 25$ s, Gao et al.'s method fails to compensate for the fault's effect and undergoes a large steady-state error. This observation is aligned with our discussion in Section 4.2. Our second-order sliding mode surface which was designed to address this steady-state error can effectively compensate for the effect of sensor fault and maintain accurate tracking. Note that Ma et al.'s method is also capable of compensating for the fault effect, but with a larger overshoot and slower convergence rate. The superiority of our method partially stems from our adaptive observer design which is able to estimate the fault effects significantly faster than the Ma et al. method as shown in Fig. 7.

Overall, the above simulation results show that our method (i) provides the ability to prescribe the performance of the trajectory-tracking error, (ii) addresses the steady-state error issue present in the Gao et al. method while maintaining similar fast convergence, and (iii) enables faster detection of fault and subsequently more effective fault compensation compared to the Ma et al. method.

5.2. Example 2: Three-Degrees-of-Freedom Robotic Manipulator

To further examine the effectiveness of the proposed method, we consider another example in which the trajectory control of a three-degrees-of-freedom manipulator is considered. This manipulator is a newly designed system to be used as a solar tracker base, as shown in Fig. 8. The model of the manipulator is given in C. More details can be found in [45].

We study the system performance under different forms of sensor faults: (i) sinusoidal in the form of $0.5(\sin t + \sin 3.5t)$ rad, (ii) an offset of 0.5 rad with additive noise, (iii) a continuously increasing fault represented by a ramp signal, and (iv) a complicated fault scenario comprised of step, ramp, and sinusoidal signals. We apply all these faults to the position sensor of all three

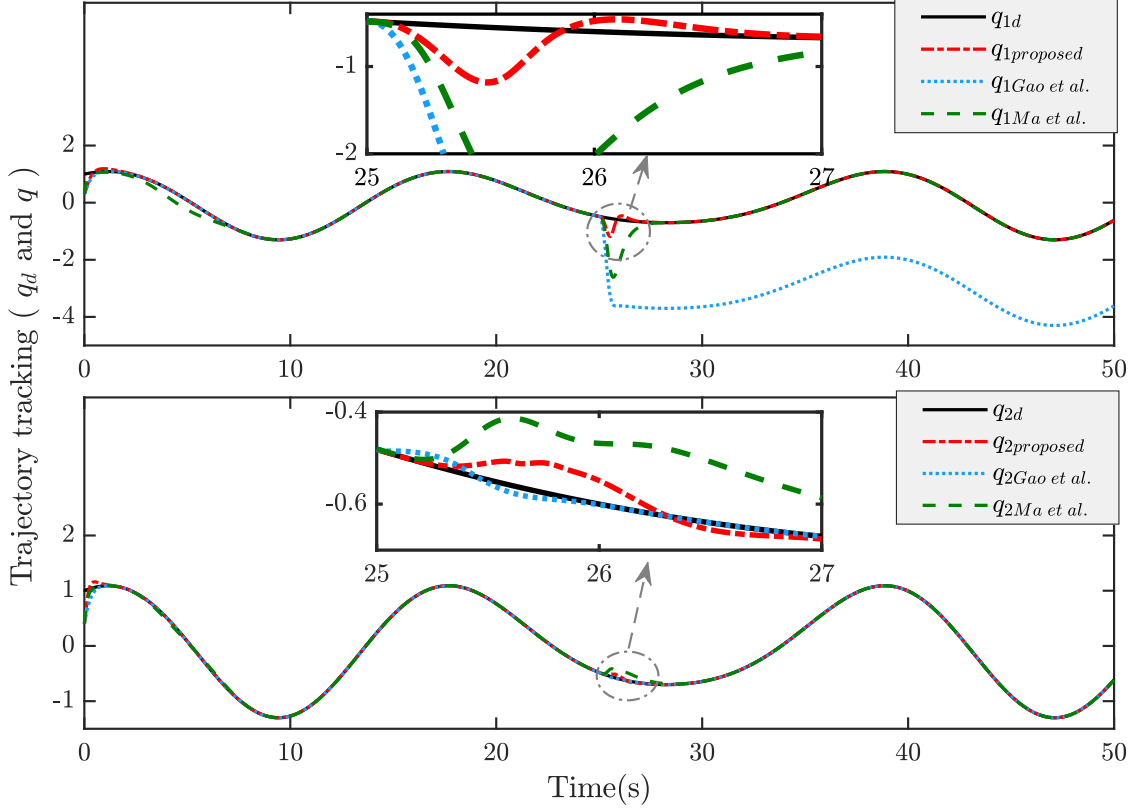


Figure 5: Time trajectory of robot joint positions for the proposed method, Gao et al. [39] and Ma et al. [7]

joints at $t = 25$ s. As mentioned in Section 1, one feature of sliding mode controllers is their inherent capability to passively deal with limited actuator faults. Although actuator fault is not the focus of this paper, to briefly explore the actuator fault tolerance of the proposed TSMC law, we introduce the following additive faults $5 \sin(10(t - 35))$, $5 \sin(5(t - 35))$, and $5 \sin(7(t - 35))$ to the actuators of the three joints in all subsequent simulations. We set the design parameters according to the values given in C. Figure 9 presents the tracking error of all three joints under different faults. It is evident that the controller has compensated for actuator faults. With the occurrence of sensor faults, the tracking error degrades momentarily; however, our proposed fault estimation and control scheme manages to recover the system states and restore zero steady-state error. Of note, even in the transient phase, the estimation error remains within the prescribed funnels.

Figure 10 illustrates the state estimation error in each simulation scenario, showing the proposed observer's effectiveness to recover system states shortly after the occurrence of faults. This performance is attributed to the ability of the observer to converge to the actual fault values shown in Fig. 11. The fault estimation part of the observer relies on two adaptive parameters $\hat{\pi}$ and $\hat{\beta}$ whose time trajectories are shown in Fig. 12. Note that since the results for different joints in each scenario are similar, we only present the results for the first joint.

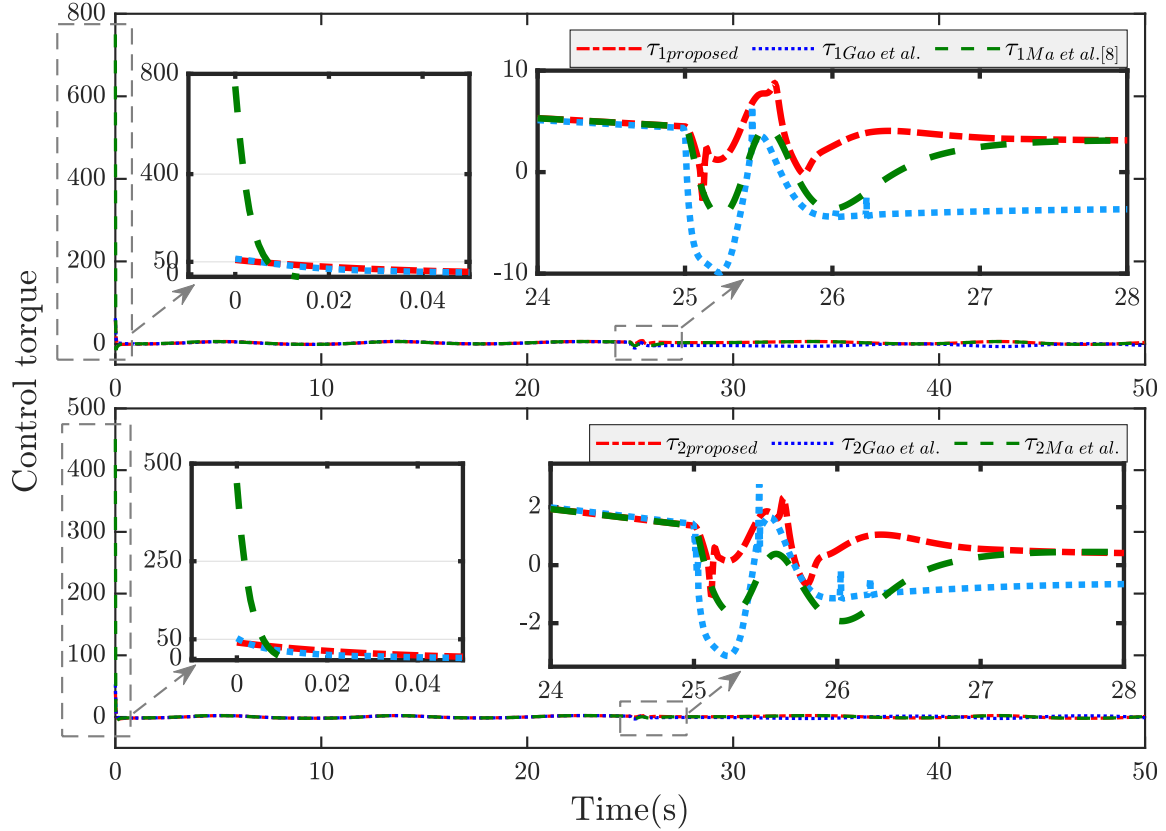


Figure 6: Control input for the proposed method, Gao et al. [39] and Ma et al. [7]

6. Conclusion

This paper presented new results for sensor fault detection and compensation in robotic manipulators. Our Lyapunov-based stability analysis and simulation experiments verified the proposed method both theoretically and numerically. Our results conclude that the representation of sensor faults as virtual actuator faults combined with adaptive observer design given in (10) can be a viable technique for sensor fault detection. In addition, the new TSMC law given in (77) proved to be effective in compensating for the sensor fault effects.

The strengths of the proposed method include the ability to detect faults without the need to impose known bounds on the fault value or its derivative, and also fault compensation with a fast and fixed-time transient response, and the ability to prescribe system performance. The above is achieved with only joint position measurements, despite many existing methods that require a measure of joint velocities in addition to position measurements.

Future research directions on the proposed method include the extension of the results to under-actuated systems, the incorporation of delays, input saturation, and/or dynamic uncertainty. For the TSMC law development, our focus was to improve upon the tracking error of the method proposed in [39] while maintaining a similar convergence speed. However, the use of non-Lipschitz functions in the control law may lead to singularity issues and oscillatory behavior of the controller. Addressing this issue can be a valuable extension of the current work. Additionally, the actuator fault tolerance properties of the TSMC law can be further explored and combined with active actuator FTC methods. Another direction to extend this work is to consider fault-tolerant coop-

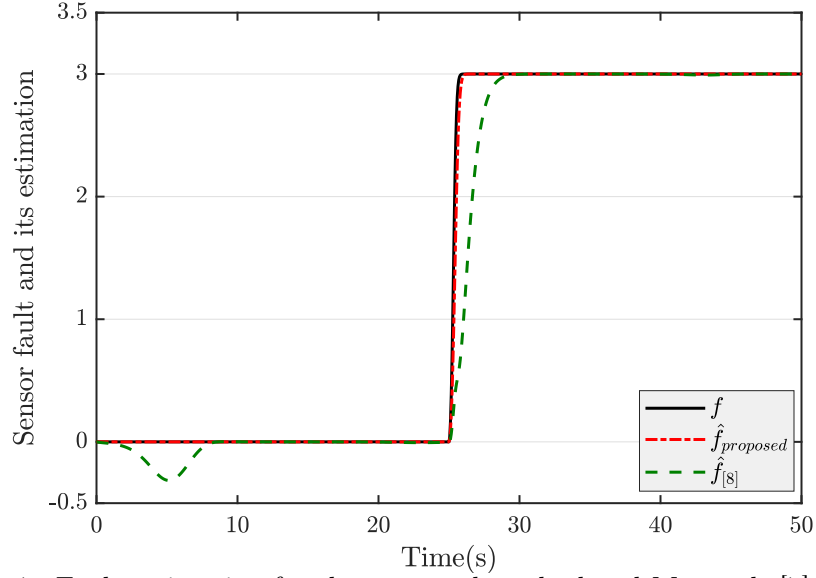


Figure 7: Fault estimation for the proposed method and Ma et al. [7]

erative control problems where multiple robotic manipulators collaborate to accomplish a task. In this context, there exist interesting observer-based results such as [46, 47] that can be leveraged to extend the current work.

Appendix A. Mathematical Background

A.1. Useful Inequalities

Lemma 1 - Young's Inequality [48]: *For any given $a, b \in \mathbb{R}^n$ we have*

$$2a^T S Q b \leq a^T S P S^T a + b^T Q^T P^{-1} Q b, \quad (86)$$

where $P > 0$, S , and Q have appropriate dimensions.

Lemma 2 [33]: *For $v = (v_1, v_2, \dots, v_n)^T \in \mathbb{R}^n$, $v_i > 0$, and the constants $0 < a_1 < 1$ and $a_2 > 1$, we have*

$$\sum_{i=1}^n v_i^{a_1} \geq \left(\sum_{i=1}^n v_i \right)^{a_1}, \quad (87)$$

and

$$\sum_{i=1}^n v_i^{a_2} \geq n^{1-a_2} \left(\sum_{i=1}^n v_i \right)^{a_2}. \quad (88)$$

Lemma 3 [49]: *Given two positive scalars a and b , we have*

$$|a| \geq 0.8814b \rightarrow 1 - 2 \tanh^2 \left(\frac{a}{b} \right) \leq 0, \quad (89)$$

and

$$|a| < 0.8814b \rightarrow 0 < 1 - 2 \tanh^2 \left(\frac{a}{b} \right) < 1. \quad (90)$$

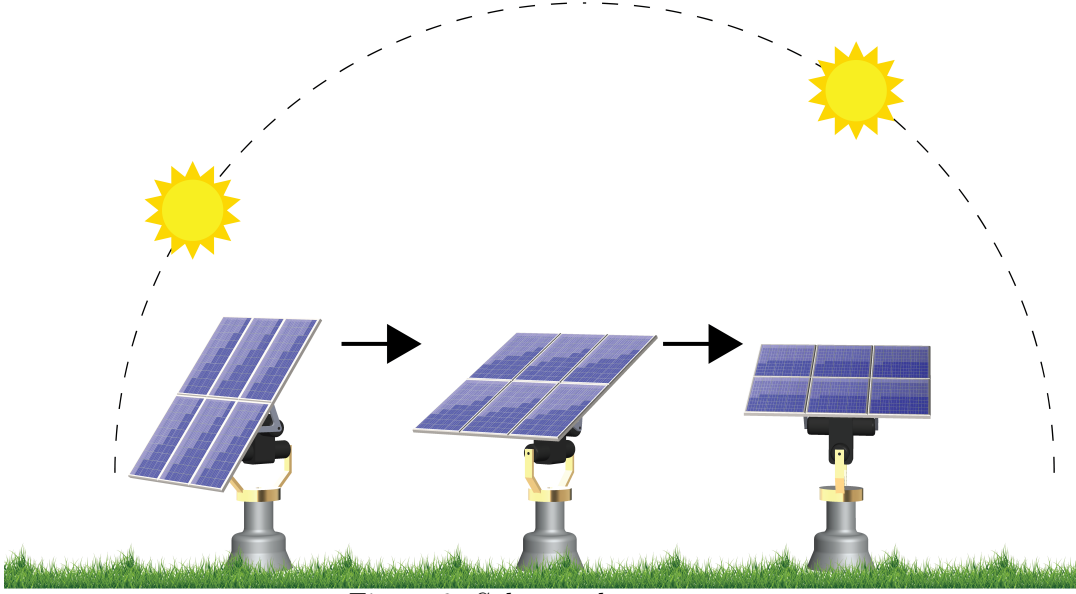


Figure 8: Solar tracker system

A.2. Ultimate Boundedness

Lemma 4: [50] *Let V and ρ be real-valued positive definite functions, and let α and β be positive constants. If they satisfy the differential inequality*

$$\dot{V} \leq -\alpha V + \beta \rho^2, \quad v(0) \geq 0, \quad (91)$$

then we have

$$V(t) \leq V(0)e^{-\alpha t} + \beta \int_0^t e^{-\alpha(t-\tau)} \rho(\tau)^2 d\tau. \quad (92)$$

A.3. Fixed-Time Stability

Lemma 5 [51]: *Consider the following nonlinear system*

$$\dot{\chi}(t) = f(\chi(t)), \quad \chi(0) = \chi_0, \quad (93)$$

where $\chi \in \mathbb{R}^n$, and $f(\chi(t)) : \mathbb{R}^n \rightarrow \mathbb{R}^n$ is a continuous function. The system (93) is said to be fixed-time stable if there exists a continuous positive definite function $V(\chi)$ such that

$$\dot{V}(\chi) \leq -a V(\chi)^\alpha - b V(\chi)^\vartheta + \zeta, \quad (94)$$

where $a > 0$, $b > 0$, $0 < \alpha < 1$, $\vartheta > 1$, and $0 < \zeta < \infty$. The convergence region is

$$\Delta = \left\{ \chi \mid V(\chi) \leq \min \left\{ \left(\frac{\zeta}{(1-\theta)a} \right)^{\frac{1}{\alpha}}, \left(\frac{\zeta}{(1-\theta)b} \right)^{\frac{1}{\vartheta}} \right\} \right\}, \quad (95)$$

where $0 < \theta < 1$, and the settling time is $T(\chi_0)$ such that $T(\chi_0) < T_{max}$, and $0 < T_{max} \leq \frac{1}{a(1-\alpha)} + \frac{1}{b(1-\vartheta)}$.

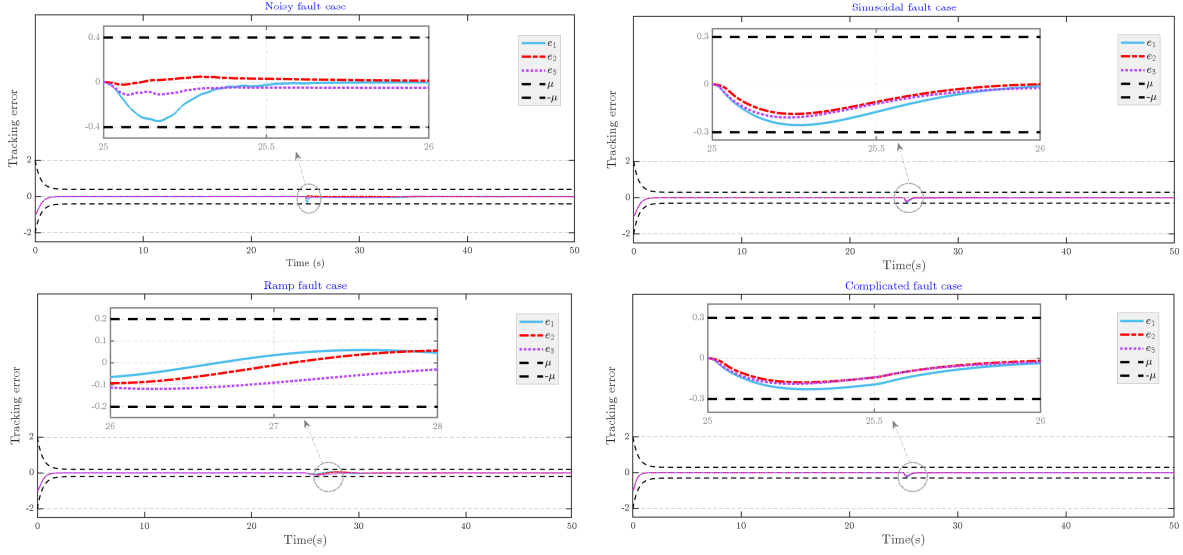


Figure 9: Tracking error in different fault scenarios

Lemma 6 [39]: *Consider the following scalar system*

$$\dot{\chi} = -\frac{1}{\varphi(\chi)} \left(\underline{\lambda} \text{sgn}^{p^*}(\chi) + \bar{\lambda} \text{sgn}^{\bar{p}}(\chi) \right), \quad (96)$$

where $\varphi(\chi) = a_1 + (1 - a_1)e^{-b_1|\chi|^{c_1}}$, $p^* = 0.5 \left(\underline{p}/\underline{q} + (\underline{p}/\underline{q} - 1) \text{sgn}(|\chi| - 1) \right)$, $\underline{\lambda} > 0$, $\bar{\lambda} > 0$, $0 < a_1 < 1$, $b_1 > 0$, c_1 is a positive even integer, and $\underline{p} > 0$, $\underline{q} > 0$, $\bar{p} > 0$, $\bar{q} > 0$, $\underline{p} > \underline{q}$, and $\bar{p} < \bar{q}$ are odd integers. The system (96) is fixed-time stable with the following convergence time

$$T_{s1}(\chi_0) < \frac{\underline{q}}{\underline{\lambda}(\underline{p} - \underline{q})} + \frac{\bar{q}}{\bar{q} - \bar{p}} \frac{1}{\bar{\lambda}} \ln \left(1 + \frac{\underline{\lambda}}{\bar{\lambda}} \right). \quad (97)$$

Appendix B. Parameters Values Used in Example 1 of Simulations

The robotic manipulator's parameters are set according to [39].

The controller parameters are set as $\underline{\lambda} = 1$, $\bar{\lambda} = 2$, $a = 0.7$, $b = 1$, $c = 2$, $\underline{p} = \bar{q} = p_\sigma = \bar{q}_\sigma = 25$, $\underline{q} = \bar{p} = \bar{p}_\sigma = q_\sigma = 23$, and $c_{1\sigma} = \bar{c}_{1\sigma} = k_{1\sigma} = 10$.

The performance prescription function parameters are set as $\mu_0 = 5$, $\mu_\infty = 2$, and $l = 0.1$ for Fig. 3, and $\mu_0 = 1$, $\mu_\infty = 0.01$, and $l = 10$ for Fig. 4.

The observer parameters are set as $\rho = 100$, $\Gamma = 0.05$, $\gamma = 1$, $\varepsilon = I_2$, $\rho_c = 0.001$,

$$A_3 = \begin{pmatrix} 20 & 0.1 \\ 0.1 & 20 \end{pmatrix},$$

$$P = \begin{pmatrix} 5.9419 & 0.0001 & -0.6670 & 0.0001 & -1.9084 & 0.0040 \\ 0.0001 & 5.9419 & 0.0001 & -0.6670 & 0.0040 & -1.9084 \\ -0.6670 & 0.0001 & 0.6044 & -0.0000 & -0.0265 & 0.0001 \\ 0.0001 & -0.6670 & -0.0000 & 0.6044 & 0.0001 & -0.0265 \\ -1.9084 & 0.0040 & -0.0265 & 0.0001 & 4.7186 & -0.0106 \\ 0.0040 & -1.9084 & 0.0001 & -0.0265 & -0.0106 & 4.7186 \end{pmatrix},$$

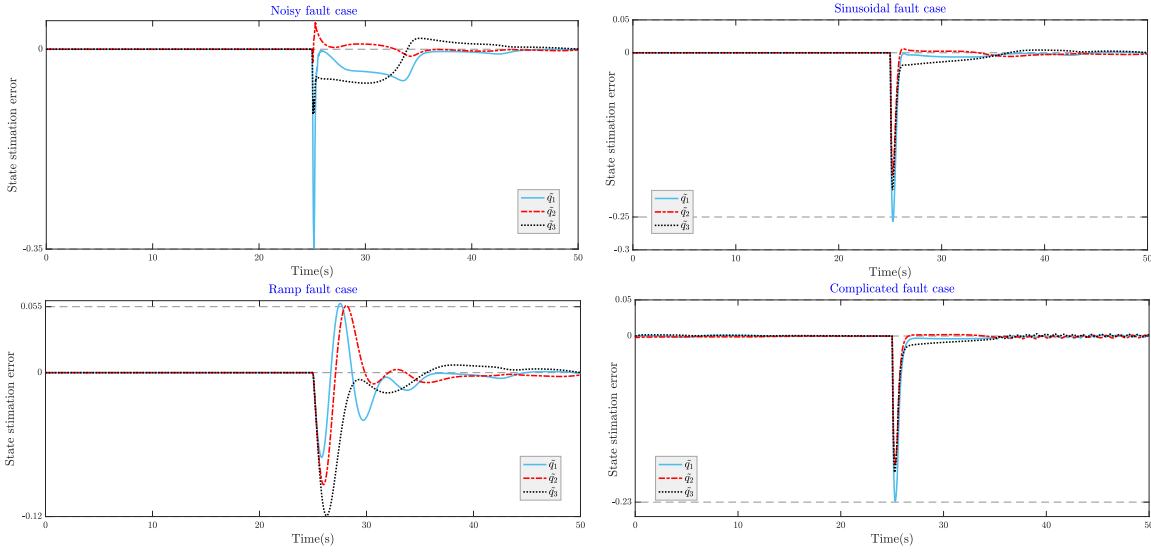


Figure 10: State estimation error in different fault scenarios

and

$$L = \begin{pmatrix} 14.1213 & 0.0036 \\ 0.0536 & 14.1214 \\ 15.2936 & 0.0015 \\ 0.0626 & 15.2936 \\ -7.2526 & -0.1340 \\ 0.0006 & -7.2528 \end{pmatrix}.$$

Appendix C. Parameters Values Used in Example 2 of Simulations

The elements of the $M(q)$ matrix include

$$m_{11} = s_2^2 (m_2 \ell_2^2 + m_3 (c_3 \ell_3 + L_2)^2 + I_{y_2} + I_{y_3}) + m_3 s_3^2 \ell_3^2 + I_{z_1} + c_2^2 (I_{z_2} + s_3^2 I_{x_3} + c_3^2 I_{z_3}),$$

$$m_{12} = m_{21} = s_3 c_2 (c_3 (I_{x_3} - I_{z_3}) - m_3 \ell_3 (c_3 \ell_3 + L_2)),$$

$$m_{13} = m_{31} = s_2 (m_3 \ell_3 (\ell_3 + c_3 L_2) - I_{y_3}),$$

$$m_{22} = m_2 \ell_2^2 + m_3 (c_3 \ell_3 + L_2)^2 + I_{x_2} + c_3^2 I_{x_3} + s_3^2 I_{z_3}$$

$$m_{23} = m_{32} = 0,$$

and

$$m_{33} = m_3 \ell_3^2 + I_{y_3}.$$

The elements of the $D(q, \dot{q})$ include

$$d_{11} = (s_3 c_3 (m_3 \ell_3^2 + c_2^2 (I_{x_3} - I_{z_3}) - s_2^2 (m_3 s_3 \ell_3 (c_3 \ell_3 + L_2))) \dot{q}_3 + s_2 c_2 (m_2 \ell_2^2 + m_3 (c_3 \ell_3 + L_2)^2 + I_{y_2} + I_{y_3} - I_{z_2} - s_3^2 I_{x_3} - c_3^2 I_{z_3}) \dot{q}_2,$$

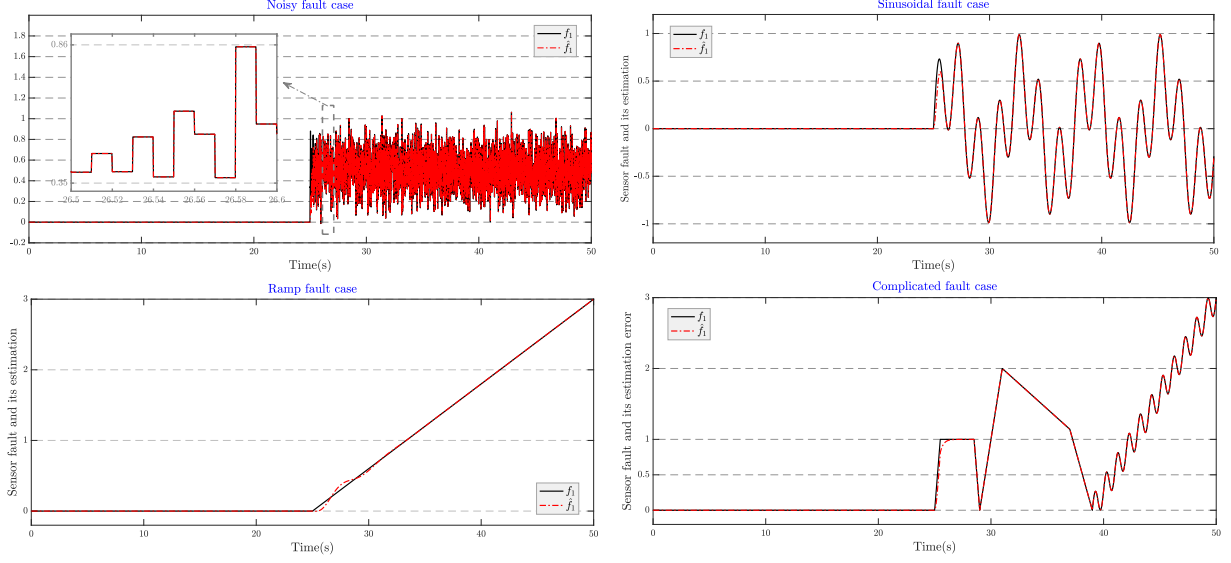


Figure 11: Sensor fault and its estimation error in different fault scenarios

$$\begin{aligned}
d_{12} &= s_2 c_2 (m_2 \ell_2^2 + m_3 (c_3 \ell_3 + L_2)^2 + I_{y_2} + I_{y_3} - I_{z_2} - s_3^2 I_{x_3} - c_3^2 I_{z_3}) \dot{q}_1 \\
&\quad - s_2 s_3 (c_3 (I_{x_3} - I_{z_3}) - m_3 \ell_3 (c_3 \ell_3 + L_2)) \dot{q}_2 \\
&\quad + c_2 (m_3 s_3^2 \ell_3^2 + c_3^2 (I_{x_3} - I_{z_3}) + \frac{1}{2} (I_{z_3} - I_{y_3} - I_{x_3})) \dot{q}_3, \\
d_{13} &= (s_3 c_3 (m_3 \ell_3^2 + c_2^2 (I_{x_3} - I_{z_3})) - s_2^2 (m_3 s_3 \ell_3 (c_3 \ell_3 + L_2))) \dot{q}_1 \\
&\quad + c_2 (m_3 s_3^2 \ell_3^2 + c_3^2 (I_{x_3} - I_{z_3}) + \frac{1}{2} (I_{z_3} - I_{x_3} - I_{y_3})) \dot{q}_2 \\
&\quad - m_3 s_2 s_3 \ell_3 L_2 \dot{q}_3, \\
d_{21} &= -s_2 c_2 (m_2 \ell_2^2 + m_3 (c_3 \ell_3 + L_2)^2 + I_{y_2} + I_{y_3} - I_{z_2} - s_3^2 I_{x_3} - c_3^2 I_{z_3}) \dot{q}_1 \\
&\quad + c_2 (c_3^2 (I_{x_3} - I_{z_3}) - m_3 c_3 \ell_3 (c_3 \ell_3 + L_2) + \frac{1}{2} (I_{y_3} + I_{z_3} - I_{x_3})) \dot{q}_3, \\
c_{22} &= s_3 (c_3 (I_{z_3} - I_{x_3}) - m_3 \ell_3 (c_3 \ell_3 + L_2)) \dot{q}_3 \\
d_{23} &= c_2 (c_3^2 (I_{x_3} - I_{z_3}) - m_3 c_3 \ell_3 (c_3 \ell_3 + L_2) + \frac{1}{2} (I_{y_3} + I_{z_3} - I_{x_3})) \dot{q}_1 \\
&\quad + s_3 (c_3 (I_{z_3} - I_{x_3}) - m_3 \ell_3 (c_3 \ell_3 + L_2)) \dot{q}_2, \\
d_{31} &= (s_2^2 (m_3 s_3 \ell_3 (c_3 \ell_3 + L_2)) - s_3 c_3 (m_3 \ell_3^2 + c_2^2 (I_{x_3} - I_{z_3}))) \dot{q}_1 \\
&\quad + c_2 (m_3 c_3 \ell_3 (c_3 \ell_3 + L_2) - c_3^2 (I_{x_3} - I_{z_3}) - \frac{1}{2} (I_{y_3} + I_{z_3} - I_{x_3})) \dot{q}_2, \\
d_{32} &= c_2 (m_3 c_3 \ell_3 (c_3 \ell_3 + L_2) - c_3^2 (I_{x_3} - I_{z_3}) - \frac{1}{2} (I_{y_3} + I_{z_3} - I_{x_3})) \dot{q}_1 \\
&\quad + s_3 (m_3 \ell_3 (c_3 \ell_3 + L_2) - c_3 (I_{z_3} - I_{x_3})) \dot{q}_2,
\end{aligned}$$

and $d_{33} = 0$, where s_i and c_i stand for $\sin(q_i)$ and $\cos(q_i)$, respectively.

The vector of the effect of gravitational force is expressed as

$$G(q) = -g \begin{pmatrix} 0 \\ s_2 (m_2 l_2 + m_3 (c_3 \ell_3 + L_2)) \\ m_3 \ell_3 s_3 c_2 \end{pmatrix}.$$

The parameter values of the robot set as $m_1 = 27.387 \text{ kg}$, $m_2 = 15.843 \text{ kg}$, $m_3 = 40.53 \text{ kg}$, $l_1 = 0.07 \text{ m}$, $l_2 = 0.085 \text{ m}$, $l_3 = 0.326 \text{ m}$, $L_1 = 0.410 \text{ m}$, $L_2 = 0.170 \text{ m}$, $L_3 = 0.5 \text{ m}$, $I_{x_1} = 0.285 \text{ kg.m}^{-2}$, $I_{x_2} = 0.254 \text{ kg.m}^{-2}$, $I_{x_3} = 2.161 \text{ kg.m}^{-2}$, $I_{y_1} = 0.458 \text{ kg.m}^{-2}$, $I_{y_2} = 0.254 \text{ kg.m}^{-2}$, $I_{y_3} = 1.949 \text{ kg.m}^{-2}$, $I_{z_1} = 0.427 \text{ kg.m}^{-2}$, $I_{z_2} = 0.229 \text{ kg.m}^{-2}$, $I_{z_3} = 3.341 \text{ kg.m}^{-2}$, and $g = 9.807 \text{ m.s}^{-2}$.

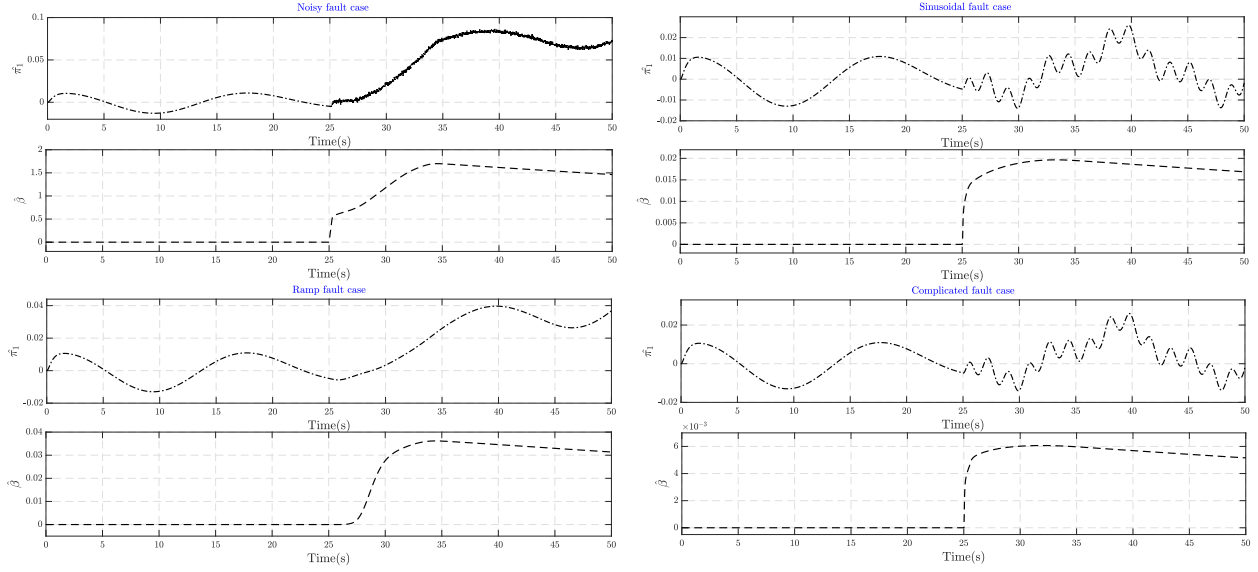


Figure 12: Time response of $\hat{\pi}_1$ and $\hat{\beta}_1$ in different fault scenarios

The controller parameters are set as $\underline{\lambda} = 0.01$, $\bar{\lambda} = 1$, $\underline{p} = \bar{q} = 11$, $\underline{q} = \bar{p} = 9$, $a = 0.7$, $b = 1$, $c = 2$, $c_{1\sigma} = \bar{c}_{1\sigma} = k_{1\sigma} = 1$, $p_\sigma = \bar{q}_\sigma = 11$, and $\bar{p}_\sigma = q_\sigma = 9$.

The performance prescription function parameters are set as $l = 2$, $\mu_0 = 2$, and $\mu_\infty = 0.3$.

The observer parameters are set as $\rho = \rho_c = \Gamma = 0.01$, $\gamma = 10$, $\varepsilon = 300I_3$, $A_3 = 100I_3$,

$$P = \begin{pmatrix} 3.23637 & 2.23e-19 & -8.10e-17 & -1.07894 & -1.88e-16 & 4.07e-17 & -0.01348 & 6.85e-17 & -9.24e-17 \\ 2.23e-19 & 3.23637 & 1.18e-15 & 3.68e-16 & -1.07894 & 3.53e-16 & -6.84e-17 & -0.01348 & -5.63e-16 \\ -8.10e-17 & 1.18e-15 & 3.23637 & -4.51e-17 & -3.99e-16 & -1.07894 & 9.07e-17 & 5.86e-16 & -0.01348 \\ -1.07894 & 3.68e-16 & -4.51e-17 & 3.237968 & -3.31e-17 & -2.92e-17 & -0.03236 & -1.35e-17 & 7.44e-19 \\ -1.88e-16 & -1.07894 & -3.99e-16 & -3.31e-17 & 3.237968 & 9.90e-16 & 3.71e-19 & -0.03236 & -1.45e-17 \\ 4.07e-17 & 3.53e-16 & -1.07894 & -2.92e-17 & 9.90e-16 & 3.237968 & 8.63e-19 & 6.08e-18 & -0.03236 \\ -0.01348 & -6.84e-17 & 9.07e-17 & -0.03236 & 3.71e-19 & 8.63e-19 & 2.696713 & -1.54e-17 & -2.94e-17 \\ 6.85e-17 & -0.01348 & 5.86e-16 & -1.35e-17 & -0.03236 & 6.08e-18 & -1.54e-17 & 2.696713 & 2.98e-17 \\ -9.24e-17 & -5.63e-16 & -0.01348 & 7.44e-19 & -1.45e-17 & -0.03236 & -2.94e-17 & 2.98e-17 & 2.696713 \end{pmatrix},$$

and

$$L = \begin{pmatrix} 93.74817 & -2.37e-15 & 1.78e-15 \\ -2.23e-15 & 93.74817 & -4.03e-14 \\ 1.69e-15 & -4.04e-14 & 93.74817 \\ 31.24764 & -1.11e-14 & 2.12e-15 \\ 4.98e-15 & 31.24764 & -1.19e-14 \\ -2.50e-16 & -3.27e-14 & 31.24764 \\ -98.6566 & 2.23e-15 & -3.08e-15 \\ -2.16e-15 & -98.6566 & -2.05e-14 \\ 3.19e-15 & 1.95e-14 & -98.6566 \end{pmatrix}.$$

References

- [1] A. A. Amin, K. M. Hasan, A review of fault tolerant control systems: advancements and applications, Measurement 143 (2019) 58–68.
- [2] F. Caccavale, A. Marino, F. Pierri, Sensor fault diagnosis for manipulators performing interaction tasks, in: 2010 IEEE International Symposium on Industrial Electronics, IEEE, 2010, pp. 2121–2126.

- [3] G. Paviglianiti, F. Pierri, F. Caccavale, M. Mattei, Robust fault detection and isolation for proprioceptive sensors of robot manipulators, *Mechatronics* 20 (1) (2010) 162–170.
- [4] C. Edwards, C. P. Tan, Sensor fault tolerant control using sliding mode observers, *Control Engineering Practice* 14 (8) (2006) 897–908.
- [5] L. M. Capisani, A. Ferrara, A. F. De Loza, L. M. Fridman, Manipulator fault diagnosis via higher order sliding-mode observers, *IEEE Transactions on industrial electronics* 59 (10) (2012) 3979–3986.
- [6] Y. Zeng, Y.-R. Xing, H.-J. Ma, G.-H. Yang, Adaptive fault diagnosis for robot manipulators with multiple actuator and sensor faults, in: *The 27th Chinese control and decision conference (2015 CCDC)*, IEEE, 2015, pp. 6569–6574.
- [7] H.-J. Ma, G.-H. Yang, Simultaneous fault diagnosis for robot manipulators with actuator and sensor faults, *Information Sciences* 366 (2016) 12–30.
- [8] M. S. Shaker, R. J. Patton, Active sensor fault tolerant output feedback tracking control for wind turbine systems via t-s model, *Engineering Applications of Artificial Intelligence* 34 (2014) 1–12.
- [9] H. Alwi, C. Edwards, Fault tolerant control using sliding modes with on-line control allocation, *Automatica* 44 (7) (2008) 1859–1866.
- [10] M. T. Hamayun, C. Edwards, H. Alwi, Design and analysis of an integral sliding mode fault-tolerant control scheme, *IEEE Transactions on Automatic Control* 57 (7) (2011) 1783–1789.
- [11] T. Wang, W. Xie, Y. Zhang, Sliding mode fault tolerant control dealing with modeling uncertainties and actuator faults, *ISA transactions* 51 (3) (2012) 386–392.
- [12] Q. Shen, D. Wang, S. Zhu, E. K. Poh, Integral-type sliding mode fault-tolerant control for attitude stabilization of spacecraft, *IEEE Transactions on Control Systems Technology* 23 (3) (2014) 1131–1138.
- [13] S. Zeghlache, K. Kara, D. Saigaa, Fault tolerant control based on interval type-2 fuzzy sliding mode controller for coaxial trirotor aircraft, *ISA transactions* 59 (2015) 215–231.
- [14] H. Mekki, O. Benzineb, D. Boukhetala, M. Tadjine, M. Benbouzid, Sliding mode based fault detection, reconstruction and fault tolerant control scheme for motor systems, *ISA transactions* 57 (2015) 340–351.
- [15] S. Zeghlache, H. Mekki, A. Bouguerra, A. Djerioui, Actuator fault tolerant control using adaptive rbfn fuzzy sliding mode controller for coaxial octotorotor uav, *ISA transactions* 80 (2018) 267–278.
- [16] H. Li, X. Lin, Robust finite-time fault-tolerant control for dynamic positioning of ships via nonsingular fast integral terminal sliding mode control, *Applied Ocean Research* 122 (2022) 103126.
- [17] M. Van, X. P. Do, M. Mavrovouniotis, Self-tuning fuzzy pid-nonsingular fast terminal sliding mode control for robust fault tolerant control of robot manipulators, *ISA transactions* 96 (2020) 60–68.

- [18] H. K. Khalil, *Nonlinear control*, Vol. 406, Pearson New York, 2015.
- [19] M. R. Faieghi, H. Delavari, D. Baleanu, A novel adaptive controller for two-degree of freedom polar robot with unknown perturbations, *Communications in Nonlinear Science and Numerical Simulation* 17 (2) (2012) 1021–1030.
- [20] M. R. Faieghi, H. Delavari, D. Baleanu, Control of an uncertain fractional-order liu system via fuzzy fractional-order sliding mode control, *Journal of Vibration and Control* 18 (9) (2012) 1366–1374.
- [21] H. Dastres, A. Mohammadi, M. Shamekhi, A neural network based adaptive sliding mode controller for pitch angle control of a wind turbine, in: *2020 11th Power Electronics, Drive Systems, and Technologies Conference (PEDSTC)*, IEEE, 2020, pp. 1–6.
- [22] S. Venkataraman, S. Gulati, Control of nonlinear systems using terminal sliding modes, *Journal of Dynamic Systems, Measurement, and Control* (1993).
- [23] M. Zhihong, X. H. Yu, Terminal sliding mode control of mimo linear systems, *IEEE Transactions on Circuits and Systems I: Fundamental Theory and Applications* 44 (11) (1997) 1065–1070.
- [24] Y. Wu, X. Yu, Z. Man, Terminal sliding mode control design for uncertain dynamic systems, *Systems & Control Letters* 34 (5) (1998) 281–287.
- [25] X. Yu, Y. Feng, Z. Man, Terminal sliding mode control—an overview, *IEEE Open Journal of the Industrial Electronics Society* 2 (2020) 36–52.
- [26] H. Komurcugil, Adaptive terminal sliding-mode control strategy for dc–dc buck converters, *ISA transactions* 51 (6) (2012) 673–681.
- [27] J.-J. Xiong, G.-B. Zhang, Global fast dynamic terminal sliding mode control for a quadrotor uav, *ISA transactions* 66 (2017) 233–240.
- [28] M. Boukattaya, N. Mezghani, T. Damak, Adaptive nonsingular fast terminal sliding-mode control for the tracking problem of uncertain dynamical systems, *Isa Transactions* 77 (2018) 1–19.
- [29] S. Yi, J. Zhai, Adaptive second-order fast nonsingular terminal sliding mode control for robotic manipulators, *ISA transactions* 90 (2019) 41–51.
- [30] H. Dastres, S. M. Ebrahimi, M. Malekzadeh, F. Gordillo, Robust adaptive parameter estimator design for a multi-sinusoidal signal with fixed-time stability and guaranteed prescribed performance boundary of estimation error, *Journal of the Franklin Institute* 360 (1) (2023) 223–250.
- [31] H. Dastres, A. Mohammadi, B. Rezaie, Adaptive robust control design to maximize the harvested power in a wind turbine with input constraint, *Journal of Renewable Energy and Environment* 7 (4) (2020) 30–43.
- [32] D. Li, H. Yu, K. P. Tee, Y. Wu, S. S. Ge, T. H. Lee, On time-synchronized stability and control, *IEEE Transactions on Systems, Man, and Cybernetics: Systems* 52 (4) (2021) 2450–2463.

- [33] Z. Zuo, Non-singular fixed-time terminal sliding mode control of non-linear systems, *IET control theory & applications* 9 (4) (2015) 545–552.
- [34] J. Ni, L. Liu, C. Liu, X. Hu, S. Li, Fast fixed-time nonsingular terminal sliding mode control and its application to chaos suppression in power system, *IEEE Transactions on Circuits and Systems II: Express Briefs* 64 (2) (2016) 151–155.
- [35] Q. Chen, S. Xie, M. Sun, X. He, Adaptive nonsingular fixed-time attitude stabilization of uncertain spacecraft, *IEEE Transactions on Aerospace and Electronic Systems* 54 (6) (2018) 2937–2950.
- [36] L. Zhang, Y. Wang, Y. Hou, H. Li, Fixed-time sliding mode control for uncertain robot manipulators, *IEEE Access* 7 (2019) 149750–149763.
- [37] Q. Chen, M. Gao, L. Tao, Y. Nan, Adaptive fixed time parameter estimation and synchronization control for multiple robotic manipulators, *International Journal of Control, Automation and Systems* 17 (9) (2019) 2375–2387.
- [38] C. Wang, X. Li, L. Cui, Y. Wang, M. Liang, Y. Chai, Tracking control of state constrained fractional order nonlinear systems, *ISA transactions* 123 (2022) 240–250.
- [39] M. Gao, L. Ding, X. Jin, Elm-based adaptive faster fixed-time control of robotic manipulator systems, *IEEE Transactions on Neural Networks and Learning Systems* (2021).
- [40] Y. Kang, L. Yao, W. Wu, Sensor fault diagnosis and fault tolerant control for the multiple manipulator synchronized control system, *ISA transactions* 106 (2020) 243–252.
- [41] D. T. Tran, H. V. Dao, T. Q. Dinh, K. K. Ahn, Output feedback control via linear extended state observer for an uncertain manipulator with output constraints and input dead-zone, *Electronics* 9 (9) (2020) 1355.
- [42] M. Yadegar, A. Afshar, M. Davoodi, Observer-based tracking controller design for a class of lipschitz nonlinear systems, *Journal of Vibration and Control* 24 (11) (2018) 2112–2119.
- [43] J. Zhang, A. K. Swain, S. K. Nguang, *Robust observer-based fault diagnosis for nonlinear systems using MATLAB®*, Springer, 2016.
- [44] H. Khebbache, M. Tadjine, S. Labiod, Adaptive sensor-fault tolerant control for a class of mimo uncertain nonlinear systems: Adaptive nonlinear filter-based dynamic surface control, *Journal of the Franklin Institute* 353 (6) (2016) 1313–1338.
- [45] S. M. Ebrahimi, B. Rezaie, M. Tavan, Identification of the three-axis pedestal using euler-lagrange method using mathematical approach, *International Journal of Modelling, Identification and Control* 42 (3) (2023) 211–225.
- [46] M. Doostmohammadian, H. Zarrabi, T. Charalambous, Sensor fault detection and isolation via networked estimation: rank-deficient dynamical systems, *International Journal of Control* 96 (11) (2023) 2853–2870.
- [47] M. Doostmohammadian, T. Charalambous, Distributed anomaly detection and estimation over sensor networks: Observational-equivalence and q -redundant observer design, in: *2022 European Control Conference (ECC)*, IEEE, 2022, pp. 460–465.

- [48] J. Wang, C. Wang, M. Xin, Z. Ding, J. Shan, Cooperative Control of Multi-Agent Systems: An Optimal and Robust Perspective, Academic Press, 2020.
- [49] H. Dastres, B. Rezaie, B. Baigzadehnoe, Neural-network-based adaptive backstepping control for a class of unknown nonlinear time-delay systems with unknown input saturation, *Neurocomputing* 398 (2020) 131–152.
- [50] M. Krstic, P. V. Kokotovic, I. Kanellakopoulos, Nonlinear and adaptive control design, John Wiley & Sons, Inc., 1995.
- [51] B. Jiang, Q. Hu, M. I. Friswell, Fixed-time attitude control for rigid spacecraft with actuator saturation and faults, *IEEE Transactions on Control Systems Technology* 24 (5) (2016) 1892–1898.